

Electronic ISSN: 1309-0267



**International Journal
of Engineering &
Applied Sciences**

**I
J
E
A
S**

IJEAS

**Volume 16, Issue 2
2024**

Published by Akdeniz University

HONORARY EDITORS

(in alphabetical order)

- Prof. Atluri, S.N.- University of California, Irvine-USA
Prof. Liew, K.M.- City University of Hong Kong-HONG KONG
Prof. Lim, C.W.- City University of Hong Kong-HONG KONG
Prof. Liu, G.R.- National University of Singapore- SINGAPORE
Prof. Nath, Y.- Indian Institute of Technology, INDIA
Prof. Omurtag, M.H. -ITU
Prof. Reddy, J.N.-Texas A& M University, USA
Prof. Saka, M.P.- University of Bahrain-BAHRAIN
Prof. Shen, H.S.- Shanghai Jiao Tong University, CHINA
Prof. Xiang, Y.- University of Western Sydney-AUSTRALIA
Prof. Wang, C.M.- National University of Singapore- SINGAPORE
Prof. Wei, G.W.- Michigan State University-USA

EDITOR IN CHIEF:

Assoc. Prof. Ibrahim AYDOGDU -Akdeniz University aydogdu@akdeniz.edu.tr

ASSOCIATE EDITORS:

Assist. Prof. Kadir MERCAN –Mehmet Akif Ersoy
University kmercan@mehmetakif.edu.tr

SECTION EDITORS:

- Assoc. Prof. Metin Mutlu Aydın – Ondokuz Mayıs University
Assoc. Prof. Mustafa Arda –Trakya University
Assist. Prof. Refik Burak Taymuş- Van 100. Yıl University
Dr. Shahin Nayyeri Amiri- Old Dominion University

EDITORIAL BOARD

(The name listed below is not Alphabetical or any title scale)

- Prof. Xinwei Wang -Nanjing University of Aeronautics and Astronautics
Asst. Prof. Francesco Tornabene -University of Bologna
Asst. Prof. Nicholas Fantuzzi -University of Bologna
Assoc. Prof. Keivan Kiani - K.N. Toosi University of Technology
Asst. Prof. Michele Baccocchi -University of Bologna
Asst. Prof. Hamid M. Sedighi -Shahid Chamran University of Ahvaz
Prof. Yaghoub Tadi Beni -Shahrekord University
Prof. Raffaele Barretta -University of Naples Federico II
Prof. Meltem ASILTÜRK -Akdeniz University *meltemasilturk@akdeniz.edu.tr*
Prof. Metin AYDOĞDU -Trakya University *metina@trakya.edu.tr*
Prof. Ayşe DALOĞLU - KTU *aysed@ktu.edu.tr*
Prof. Oğuzhan HASANÇEBİ - METU *oguzhan@metu.edu.tr*
Asst. Prof. Rana MUKHERJİ - The ICFAI University
Assoc. Prof. Baki ÖZTÜRK - Hacettepe University
Assoc. Prof. Yılmaz AKSU -Akdeniz University
Assoc. Prof. Hakan ERSOY- Akdeniz University
Assoc. Prof. Mustafa Özgür YAYLI -Uludağ University
Assoc. Prof. Selim L. SANİN - Hacettepe University
Asst. Prof. Engin EMSEN -Akdeniz University
Prof. Serkan DAĞ - METU
Prof. Ekrem TÜFEKÇİ - İTÜ

ABSTRACTING & INDEXING



IJEAS provides unique DOI link to every paper published.

EDITORIAL SCOPE

The journal presents its readers with broad coverage across some branches of engineering and science of the latest development and application of new solution algorithms, artificial intelligent techniques innovative numerical methods and/or solution techniques directed at the utilization of computational methods in solid and nano-scaled mechanics.

International Journal of Engineering & Applied Sciences (IJEAS) is an Open Access Journal

International Journal of Engineering & Applied Sciences (IJEAS) publish original contributions on the following topics:

Civil Engineering: numerical modelling of structures, seismic evaluation, experimental testing, construction and management, geotechnical engineering, water resources management, groundwater modelling, coastal zone modelling, offshore structures, water processes, desalination, waste-water treatment, pavement and maintenance, transport and traffic, laser scanning, and hydrographic surveying, numerical methods in solid mechanics, nanomechanic and applications, microelectromechanical systems (MEMS), vibration problems in engineering, higher order elasticity (strain gradient, couple stress, surface elasticity, nonlocal elasticity)

Electrical Engineering: artificial and machine intelligence and robotics, automatic control, bioinformatics and biomedical engineering, communications, computer engineering and networks, systems security and data encryption, electric power engineering and drives, embedded systems, Internet of Things (IoT), microwaves and optics.

Engineering Mathematics and Physics: computational and stochastic methods, optimization, nonlinear dynamics, modelling and simulation, computer science, solid state physics and electronics, computational electromagnetics, biophysics, atomic and molecular physics, thermodynamics, geophysical fluid dynamics, wave mechanics, and solid mechanics.

Mechanical Engineering: machine design, materials science, mechanics of materials, manufacturing engineering and technology, dynamics, robotics, control, industrial engineering, ergonomics, energy, combustion, heat transfer, fluids mechanics, thermodynamics, turbo machinery, aerospace research, aerodynamics, and propulsion.

IJEAS allows readers to read, download, copy, distribute, print, search, or link to the full texts of articles.



CONTENTS

Performance Evaluation of a Solar Photovoltaic (PV) Module at Different Solar Irradiance

By Anas Bala, Moshood Babatunde Alao, Aliu Olamide Oyedun, Oluwaseyi Omotayo Alabi, Mohammed Adamu 63-75

The Effects of Animal Bone Ash on Asphalt Pavement Mixtures

By Burak Öntaş, Jülide Öner 76-93

Determination of Ship Length and Draft on the Planning Stage of Cruise Ports in Türkiye

By Alp Küçükosmanoğlu 94-103

Exploring the Spatial Distribution of Coastal Drainage Basins in Turkey

By Özen Arlı Küçükosmanoğlu 104-115



Performance Evaluation of a Solar Photovoltaic (PV) Module at Different Solar Irradiance


Anas Bala ^{1*}, Babatunde Moshood Alao ², Aliu Olamide Oyedun ³, Oluwaseyi Omotayo Alabi ⁴,
Mohammed Adamu ¹

¹ Department of Mechanical Engineering, Nigerian Army University Biu, Nigeria

² Department of Mechanical Engineering, University of Ilorin, Ilorin, Nigeria

³ Institute of Waste Water Management and Water Protection Hamburg University of Technology, Hamburg, Germany

⁴ Department of Mechanical Engineering, Lead City University, Ibadan, Nigeria

✉: anas.bala@naub.edu.ng : 0000-0002-7420-2786 ^{1*}, 0009-0006-6819-5870 ², 0000-0001-5845-4302 ³, 0009-0005-0027-5930 ⁴, 0009-0003-0527-8431 ⁵

Received: 02.02.2024, Revised: 14.04.2024, Accepted: 22.04.2024

Abstract

The primary constraint of photovoltaic (PV) systems is the relatively low conversion efficiency of PV panels (PVPs), heavily influenced by their operating temperature and sun irradiation under various configurations. The lack of precision in accounting for PV panel temperature and solar irradiation levels heightens the financial risk associated with system installation. This study examines the impact of solar irradiation, under constant temperature conditions 25°C, on a monocrystalline PV panel under standard test conditions (STC) of Ilorin, North Central Nigeria. The output performance of a specific PV panel model was initially investigated by simulating it using the Scilab Xcos™ software. The current-voltage (I-V) and power-voltage (P-V) curves are utilized to evaluate the performance of PV panels, taking into account the temperature of the panels and varying solar irradiation levels. The simulation's findings demonstrate that when solar irradiation varies from 400 W/m² to 1000 W/m², there is a linear increase in both the open circuit voltage (Voc) and short circuit current (Isc). The amount of solar irradiance causes this linear increase. The results also revealed that the quantity of irradiation the PV modules are able to extract directly relates to the PV module's output power. Furthermore, the current and voltage reached their peak levels of 7.12 A and 15 V, respectively, when the solar radiation intensity was 1000W/m². Their minimum values were 2.95 A and 14 V, respectively, when exposed to a solar radiation of 400W/m². The power output of the photovoltaic (PV) panel grew in direct proportion to the rise in solar radiation. Specifically, the power output declined to 85.95 W when the solar radiation was 400W/m², while it was 223.64 W when the solar radiation was 1000W/m².

Keywords: PV system, Irradiance, Monocrystalline, Short circuit, Open circuit, Power

1. Introduction

Globally power demand is steadily rising but there with limited fossil energy supply. This is a worrisome trend in the energy business as suppliers tend to look for alternative sources to offer clients to stay in business therefore, there is an urgent need for a proper energy mix. Renewable energy like solar and bioenergy plays key roles in the structural supply chain of the energy mix. Fossil energy reserves have been gradually depleting yet continuously harnessed. The fossil energy exploration like crude oil severely harmed the ecosystem and over time, increased global warming[1]. The PV systems harness solar radiation as an energy source. Using cells, it converts solar radiation into a more useful energy which is electricity. At varying efficiency ranges of 7% to 40%, the PV cells produce electricity from solar radiation[1]. The



semiconductor types used for PV cell production mostly influence its conversion. PV panels typically account for the largest share of the investment cost when compared to other installation components for PV systems[2]. Therefore, making reasonable returns after investing in this system heavily relies on PV panels' (PVP's) power generation capacity. Sadly, a few deteriorating factors frequently result in low conversion efficiency for PVP's. PV panel temperature is recognized as a key component in energy production forecasting[3]. For instance, extended high-temperature and operating conditions may cause a PVP's capacity to produce power to deteriorate permanently[4]. The elevated temperature is caused by wasted energy that is created as a result of absorbing solar energy. A PVP's can mostly convert about 20% of solar radiation into electricity[2]. Most of what is still present is converted to heat. The PVP's working temperature is increased due to the stored heat energy, which reduces the panel's electrical efficiency[5]. According to standard test condition (STC), a PVP's conversion efficiency decreases by 0.40 to 0.50% for every degree of temperature increase[6].

Silica is the main component of most solar cells. The electrons that are flowing through the solar PV material because of sunlight hitting a cell are converted into direct current (DC) electricity. By attaching an inverter to the system, the DC is transformed into AC, and the AC electricity is then fed into household devices as electric power[5]. Many materials including copper and cadmium telluride are used in making PV cells. There are, however, three silicon-based materials including monocrystalline (MCS), polycrystalline (PCS), and amorphous (APS) widely used in solar PV cells[7]. Highly concentrated photovoltaic (HCPV) systems focus solar energy onto tiny solar cells using optical devices (lenses or mirrors)[8]. According to the manufacturer of semiconductor materials, there are more efficient new forms of PV modules which are about 31.8% better than the ones previously produced[9]. Just like other technologies, in the last three decades, solar cell efficiency has increased steadily. This ranges from 16.5% CdTe, 18.4% CIGS, 24.7% c-Si, to 39% GaInP/GaAs/Ge[1].

In the past decade, numerous research have investigated the impact of solar radiation fluctuations and temperature volatility on the performance of photovoltaic (PV) panels. Suwapaet and Boonla's[10] research shows that AMS solar panels outperform MCS panels operating at elevated temperatures. Also, MCS panels supplied produce smaller power when compared to AMS at 600 W/m² range, despite no appreciable changes in PV panel temperature[10]. However, the targeted output size is below the expected efficiency of 31%, 50% and 54-68% for single junction, 3-cell stacks and hot carriers respectively. Only commercial modules had achieved efficiencies of 50% to 65% of these "champion" cells[10]. Ike[11] explored the impact of weather factors, such as ambient temperature, on the total efficiency of solar panels. The author asserted that there exists an inverse relationship between the ambient temperature and the output energy of the system. Additionally, the study emphasized the need to ensure proper airflow through the panels during the design process. Dash and Gupta[12] examined the correlation between temperature and the electrical output generated by various solar panels. The authors employed the temperature coefficient as a benchmark function for photovoltaic (PV) output power. The study determined that monocrystalline panels had the most average power loss, with a value of 0.446% per degree Celsius. Swapnil et al.[13] after conducting a thorough analysis of numerous research, it was shown that there is a direct correlation between temperature and both the photoelectric conversion efficiency and the output power of photoelectric modules. The researcher demonstrated that numerical parameters are contingent upon both the substance and the system simultaneously.

Chander et al.[14] used a solar simulator to research the effects of varying PV cell temperature during steady-state lighting conditions. This study discovered that the PV cell's temperature substantially impacts output parameters. It was discovered that the I_{sc} had positive coefficients

for temperature, while other parameters like V_{oc} negatively impacted the temperature coefficients. The temperature impact on power with varying PV panels is reported by researchers[2], [11]. The mean power loss of monocrystalline PV panels when the temperature coefficient was considered was -0.45% per °C. Khaled et al.[15] examined the impact of shadowing on the peak power production of the photovoltaic (PV) panels and the resulting reduction in efficiency. The study determined that raising the temperature of the photovoltaic (PV) system leads to a decrease in its maximum output power. Based on the report by Temaneh-Nyah and Mukwekwe[16] elevated temperatures caused PV panels to lose power. Their findings also showed high temperatures caused a median energy waste of 37.8 kW for PV system installations for its regular 12-hour operations, which is 14.6 kWh [16]. The coefficient of temperature was found to be about 0.31% of lost energy per Kelvin [16]. Various kinds of PV panel technologies have produced output power in a variety of ways because of how sensitive they are to operating temperature and solar irradiance. Zhe et al.[17] examined the impact of altering solar radiation intensity on the properties and efficiency of photovoltaic (PV) modules.

A number of researchers have employed mathematical models to accurately forecast the impact of variables, such as radiation intensity and temperature, across various global locations and the accuracy of the results is confirmed by comparing them to the results of real-world tests Al-Waeli et al. [18]

The present study examines the impact of variations in solar radiation and constant temperature on the overall efficiency of solar panels. An investigation was conducted to examine the connections between these variables and fundamental characteristics of photovoltaic (PV) panels, including short circuit current, open circuit voltage, output power, and efficiency. While there may exist several international studies resembling this particular study, they pertain to the conditions of different countries rather than the weather conditions specifically in Nigeria, particularly in the city of Ilorin, the capital. Ilorin exhibits a continental climate, with scorching temperatures during the summer and frigid conditions during the winter. This city experiences periodic fluctuations in relative humidity, however they are restricted in magnitude. Additionally, the wind velocity remains consistently mild, seldom surpassing 3 m/s on the majority of days throughout the year. To the best of the researchers' knowledge, no previous study of this nature has been done either domestically or abroad. The first section of this article provides background information to the research study while Section 2 provides information about the PV module's specifications. In section 3, *Scilab XcosTM* software analyzed solar irradiance effects on the study's PV module. However, section 4 discusses all the simulation's findings and results were further discussed.

2. Materials and Method

Firstly, a PV module can be arranged in series and or parallel. This corresponding arrangement gives the expected current and voltage output. In this study the analysis of the PV panel output performance was simulated using *Scilab XcosTM* simulation software. By using this software, the basic data of PV panel can be explored as shown in Table 2. All data were determined under standard test conditions (STC) of Ilorin, North Central Nigeria with a rating of 25 °C, and a range of solar irradiance between 400W/m² and 1000W/m². Due to the highly unrealistic nature of the normal test settings, different data were inputted that closely resemble the actual operating conditions. The simulation programme yielded several key data points, including short circuit current, output power, open circuit voltage, and efficiency. Crucial connections can be identified to assess the overall effectiveness of PV panels, such as the correlation between efficiency and solar radiation intensity and temperature, the link between voltages and

current, the relationship between voltages and output power, and other less significant connections.

The purpose of the simulation is to observe the effect of solar irradiance on PV panel output performance at constant temperature. After all parameters have been identified, the next method is to analyze the PV panel performance through the characteristics of current-voltage (I-V) and power-voltage (P-V) curves based on different amount of solar irradiance. To model the electrical characteristics in a PV module in predicting the power output, five important relevant equations need to be solved. These equations are:

i. Photo-current (I_{ph})

$$I_{ph} = [I_{sc} + k_i \cdot (T - 298)] \cdot \frac{G}{1000} \quad (1)$$

ii. Saturation current (I_o)

$$I_o = I_{rs} \cdot \left[\frac{T}{T_n} \right]^3 \cdot \exp \left[\frac{q \cdot E_{go} \cdot \left(\frac{1}{T_n} - \frac{1}{T} \right)}{n \cdot K} \right] \quad (2)$$

iii. Reverse saturation current (I_{rs})

$$I_{rs} = \frac{I_{sc}}{e^{\left(\frac{q \cdot V_{oc}}{n \cdot N_s \cdot K \cdot T} \right) - 1}} \quad (3)$$

iv. Current through shunt resistor (I_{sh})

$$I_{sh} = \left(\frac{V + I \cdot R_s}{R_{sh}} \right) \quad (4)$$

v. Output current (I)

$$I = I_{ph} - I_o \cdot \left[\exp \left(\frac{q \cdot (V + I \cdot R_s)}{n \cdot K \cdot N_s \cdot T} \right) - 1 \right] - I_{sh} \quad (5)$$

Equations 1, 2 and 3 above represent the Photo-current (I_{ph}) which is the output current, Saturation current (I_o) and Reverse saturation current (I_{rs}) respectively. These equations utilizes the constant values in order to produce specified output used in the block diagram as shown in Figs. 2, 3 and 4 respectively. Equations 4 and 5 will provide the current (I) and voltage (V) which are the two most important parameters of interest required by a PV module. There are numerous software that could be used to solve these equations. However, this study employed the use of Scilab XcosTM for the modeling and simulation of these complex equations. This study used this simulation tool because of its robustness in solving such complex equations [15]. For mathematical modeling and simulation of the PV module in Scilab XcosTM, Table 1 shows the required parameters used in the five equations previously mentioned.

Table 1. Photovoltaic (PV) module constants and variables

Designation (Unit)	Value
I_{ph} photo – current (A)	I_{ph}
I_{sc} short circuit current (A)	I_{sc}
k_i short – circuit current of cell at 25°C and 1000 W/m ²	0.0032
T operating temperature (K)	T
T_n nominal temperature (K)	298
G solar irradiation (W/m ²)	G
Q electron charge (C)	1.6×10^{-19}
V_{oc} open circuit voltage (V)	V_{oc}
N the ideality factor of the diode	1.3
K Boltzmann’s constant (J/K)	1.38×10^{-23}
E_{go} band gap energy of the semiconductor (eV)	1.1
N_s number of cells connected in series	N_s
N_p number of PV modules connected in parallel	N_p
R_s series resistance (Ω);	0.221
R_{sh} shunt resistance (Ω);	415.405
V_t diode thermal voltage (V)

The module rating showing the characteristics of a solar cell obtained from a Manufacturer’s Datasheet [19] that will be used for modeling in Xcos™ is shown in Table 2.

Table 2. Data obtained/estimated from Mitsubishi PV-TJ225GA6 at (STC) [19]

Designation	Rating
Maximum power rating (P_{mp})	225 W
Minimum power rating (P_{mp})	218.3 W
Tolerance of maximum power rating	+3/–3%
Voltage at maximum power (V_{mp})	30.0 V
Current at maximum power (I_{mp})	7.50 A
Open circuit voltage (V_{oc})	36.4 V
Short circuit current (I_{sc})	8.30 A
Total number of cells in series (N_s)	60
Total number of cells in parallel (N_p)	1

The Fig. 1 shows the module’s circuit representation.

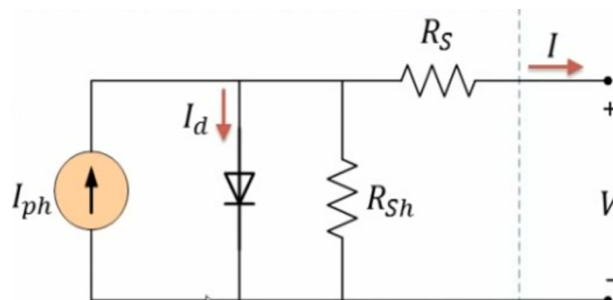



Fig. 1: Photovoltaic (PV) module cell circuit [20]

In modeling and simulating the PV module using Scilab Xcos™ with the manufacturer’s specifications in Table 2, the following steps are taken:

Step one: Launch Xcos

Firstly Scilab needs to be launched, then launch Xcos from the general environment using  symbol or by searching for Xcos. By default, Xcos opens with two windows, a palette browser and an editing window.

Step two: Set Context

The next step is specifying in Scilab user’s parameters. This is where values from Table 2 (i.e. Manufacturer’s Specification) will be specified. This will be done from the editing window menu bar, in Simulation/Set Context.


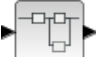




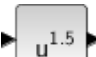
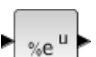
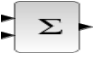




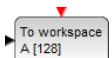
Step three: Blocks Arrangement

Instead of arranging the blocks in the editing window for the whole diagram (i.e. the five equations in block form) on one page, they can be built in small pieces in superblocks.

Step four: Modeling and Simulation

The data from Scilab Xcos™ were exported to Excel. In the palette browser, the blocks shown in Table 3 were used for the exercise:

Table 3. Set of predefined blocks

Designation	Representation	Sub_Palette
Constant		Sources/CONST_m
Superblock		Port & Subsystem/SUPER_f
Ramp		Sources/RAMP
Input		Port & Subsystem/IN_f
Output		Port & Subsystem/OUT_f
Delay		Discrete time systems/DELAY_f
Power		Mathematical Operations/POWBLK_f
Exponential		Mathematical Operations/EXPBLK_m
Summation		Mathematical Operations/BIGSOM_f
Product		Mathematical Operations/PRODUCT
Clock		Sources/Clock_c
Visualization		Sinks/CSCOPXY
Mux		Recently Used Blocks/MUX_f
Matrix		Sinks/TOWS_c

Now to start arranging the blocks for each of the equation one after the other:

i. Photo-current (I_{ph})

$$I_{ph} = [I_{sc} + k_i \cdot (T - 298)]. \frac{G}{1000} \quad (6)$$

The output current is described by I_{ph} , the equation inputs are T and G with I_{sc} and k_i as constants. Fig. 2 shows the block structure for the equation.

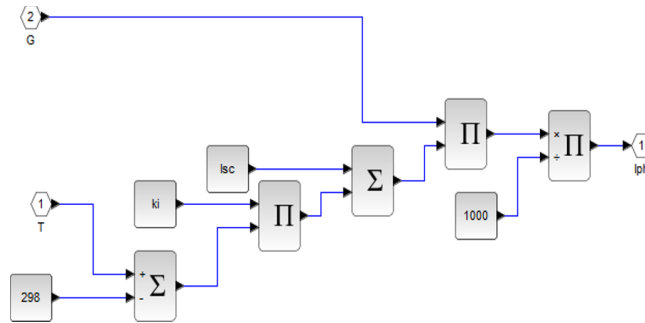


Fig. 2. Photo-current (I_{ph}) block diagram

ii. Saturation current (I_o)

$$I_o = I_{rs} \cdot \left[\frac{T}{T_n} \right]^3 \cdot \exp \left[\frac{q \cdot E_{go} \cdot \left(\frac{1}{T_n} - \frac{1}{T} \right)}{n \cdot K} \right] \quad (7)$$

In this equation I_o is specified as the output, T and I_{rs} are respective inputs. Also, the constants are T_n , q, E_{go} , n and K. Fig. 3 shows the block structure for the equation.

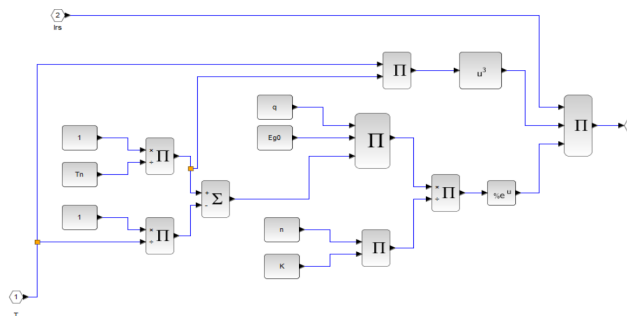


Fig. 3. Saturation current (I_o) block diagram

iii. Reverse saturation current (I_{rs})

$$I_{rs} = \frac{I_{sc}}{e^{\left(\frac{q \cdot V_{oc}}{n \cdot N_s \cdot K \cdot T} \right) - 1}} \quad (8)$$

In this equation I_{rs} and T are specified as the respective output and input. Other parameters like I_{sc} , V_{oc} , q, n, N_s and K represent constants within the equation. Fig. 4 shows the block structure for this equation.

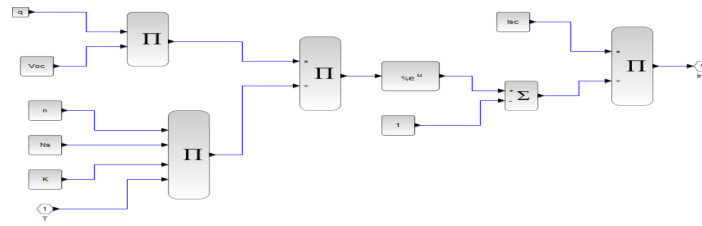


Fig. 4. Block diagram for I_{rs}

iv. Current through shunt resistor (I_{sh})

$$I_{sh} = \frac{(V + I.R_s)}{R_{sh}} \tag{9}$$

In this equation I_{sh} is specified as the output, and I and V as input with R_s and R_{sh} as the equation constants. Fig. 5 shows the block structure for the equation.

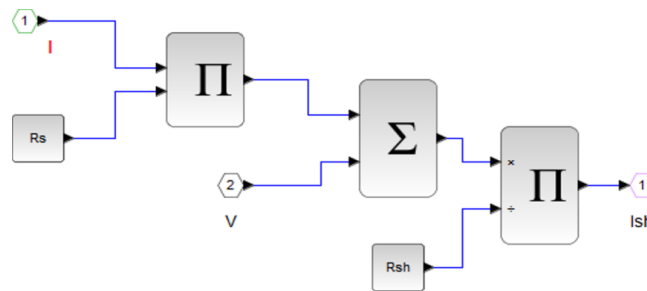


Fig. 5. Block diagram for I_{sh}

v. Output current (I)

$$I = I_{ph} - I_o \cdot \left[\exp\left(\frac{q \cdot (V + I.R_s)}{n \cdot K \cdot N_s \cdot T}\right) - 1 \right] - I_{sh} \tag{10}$$

In this equation V , T , I_o , I_{ph} and I_{sh} are specified as the inputs, with q , R_s , n , K , and N_s as the equation constants. Fig. 6 shows the block structure for the equation.

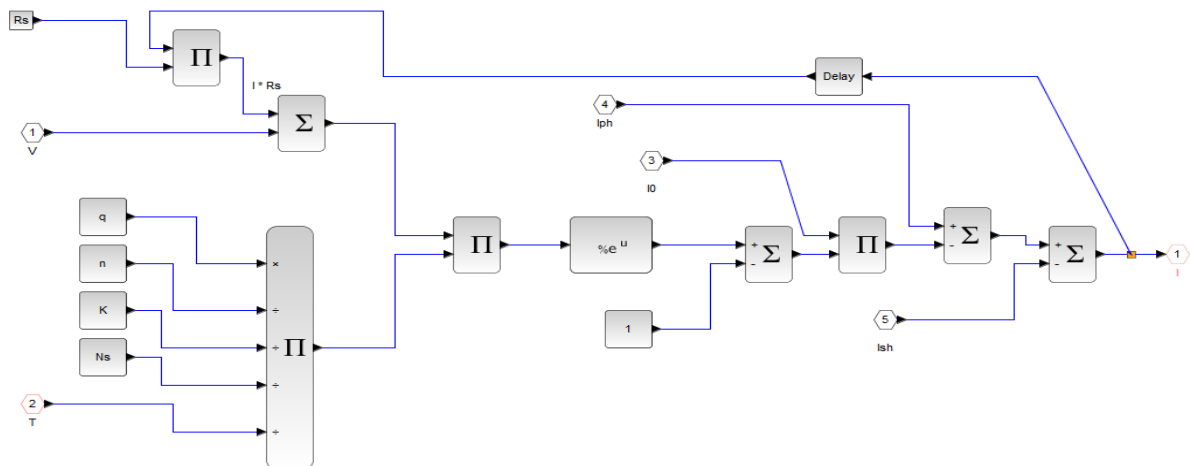


Fig. 6. Block diagram for the output current (I)

These individual blocks are connected to form a superblock in Fig. 7.

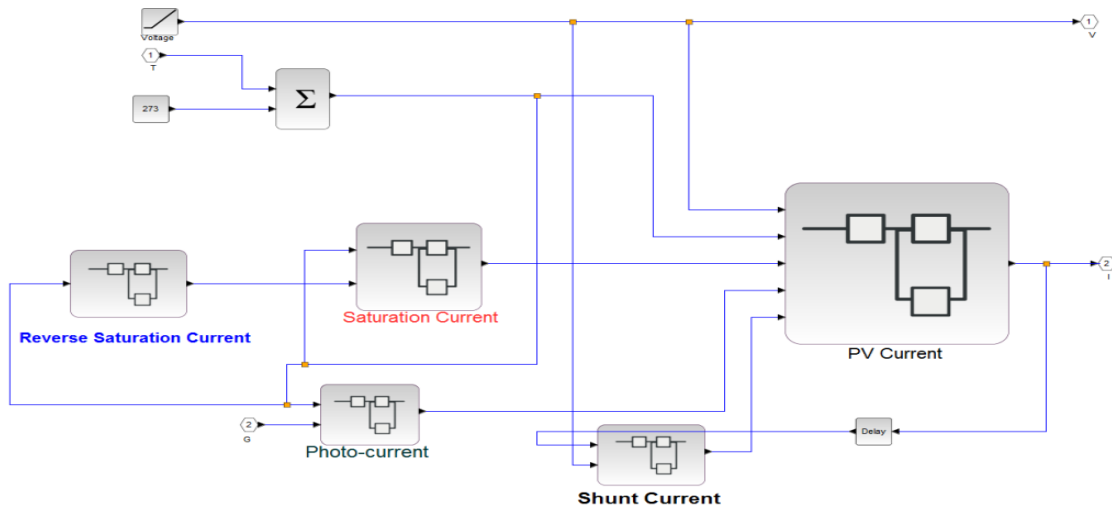


Fig. 7. Photovoltaic (PV) module sub-superblocks

For the system to produce the expected power output, certain T and G as seen in Fig. 8 are required in the system. Next section of this study shall discuss the results of modeling and simulation of the photovoltaic (PV) module.

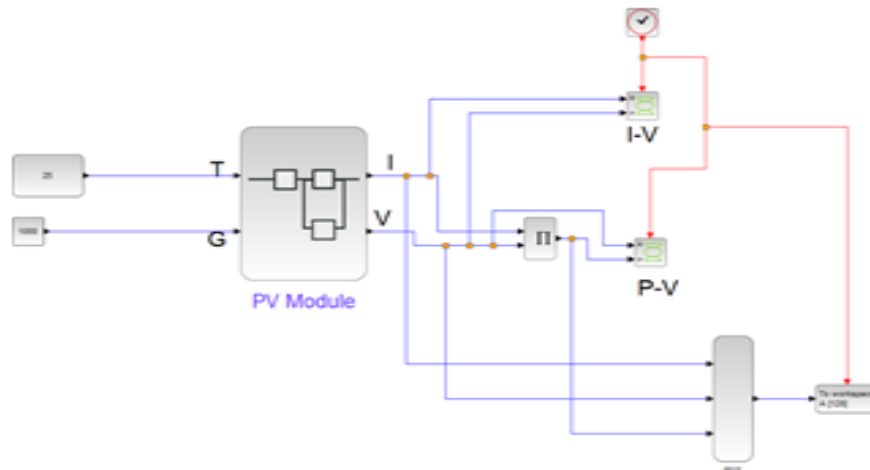


Fig. 8. Photovoltaic (PV) Module Visualization

3. Results and Discussion

The results obtained using Scilab Xcos™ were exported to Excel Worksheet as shown in Table 4. The modeling and simulation operating parameters at various sun irradiances are displayed in Table 4. The results shows that, the increase in I_{sc} through the open circuit of the PV module grows at a constant voltage, which increases the output power in the PV modules due the increase in the amount of solar in irradiance. In contrast, the output power in the PV modules rises sequentially as the voltage across their circuit increased. Also, the results further revealed that the current drops as the time interval increases. These data were used to generate a P-V vs. I-V curves at varying solar irradiance as shown in Figure 9 which was also used for the performance analysis of this study

Table 4. Inputs and Outputs Parameters after Modeling and Simulation

Solar Irradiance		@ 400 W/m ²		@ 600 W/m ²		@ 800 W/m ²		@ 1000 W/m ²	
Time [s]	V [volt]	I [amps]	P [watt]	I [amps]	P [watt]	I [amps]	P [watt]	I [amps]	P [watt]
0.1	1	3.317593	3.317593	4.977593	4.977593	6.637593	6.637593	8.297593	8.297593
0.3	3	3.312778	9.938333	4.972778	14.91833	6.632778	19.89833	8.292778	24.87833
0.5	5	3.307962	16.53981	4.967962	24.83981	6.627962	33.13981	8.287962	41.43981
0.7	7	3.303146	23.12202	4.963146	34.74202	6.623146	46.36202	8.283146	57.98202
0.9	9	3.298325	29.68492	4.958325	44.62492	6.618325	59.56492	8.278325	74.50492
1.1	11	3.291717	36.20889	4.950827	54.45909	6.609934	72.70928	8.26904	90.95944
1.3	13	3.286841	42.72893	4.945937	64.29718	6.60503	85.86538	8.264117	107.4335
1.5	15	3.281853	49.2278	4.940914	74.11372	6.599965	98.99947	8.259001	123.885
1.7	17	3.276568	55.70166	4.935535	83.90409	6.594471	112.106	8.253371	140.3073
1.9	19	3.270474	62.13901	4.929183	93.65448	6.58781	125.1684	8.246339	156.6804
2.1	21	3.262189	68.50597	4.920201	103.3242	6.577991	138.1378	8.235514	172.9458
2.3	23	3.247964	74.70316	4.904087	112.794	6.559609	150.871	8.21441	188.9314
2.5	25	3.217635	80.44089	4.868638	121.716	6.518012	162.9503	8.165432	204.1358
2.7	27	3.143669	84.87906	4.780794	129.0814	6.413507	173.1647	8.040921	217.1049
2.9	29	2.951446	85.59193	4.550969	131.9781	6.138536	178.0175	7.71175	223.6408
3.1	31	2.438846	75.60422	3.936524	122.0322	5.401835	167.4569	6.828297	211.6772
3.3	33	1.058938	34.94494	2.281105	75.27646	3.415813	112.7218	4.445613	146.7052

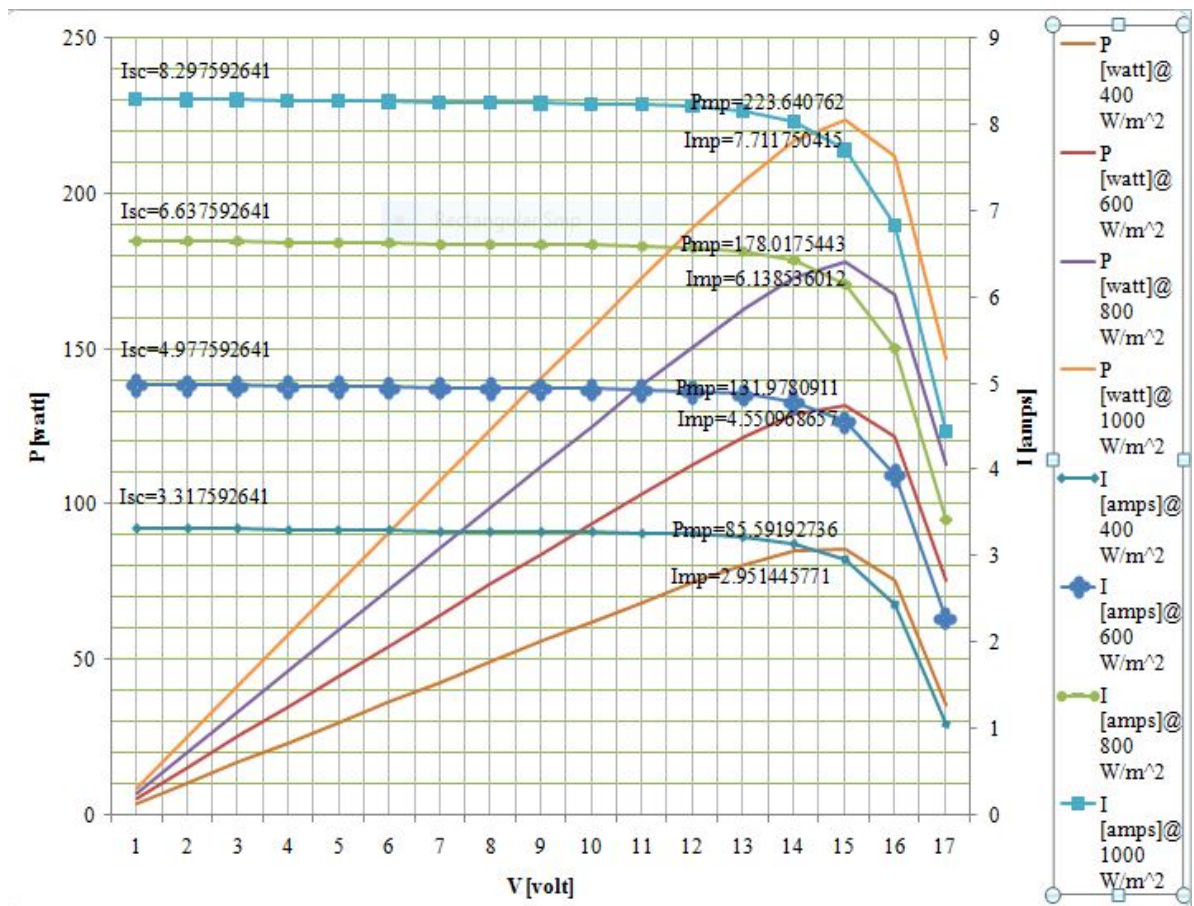


Fig. 9. Variation in (P-V) and (I-V) curves at varying solar irradiance

Figure 9 illustrates the correlation between the current, voltage, and output power under a consistent temperature of 25 °C and a fluctuating solar radiation ranging from 1000 W/m² to 400W/m². This is a theoretical scenario that cannot be implemented under actual operational circumstances. The current and voltage reached their peak levels of 7.12 A and 15 V,

respectively, when the solar radiation intensity was $1000\text{W}/\text{m}^2$. Their minimum values were 2.95 A and 14 V, respectively, when exposed to a solar radiation of $400\text{W}/\text{m}^2$. The power output of the photovoltaic (PV) panel grew in direct proportion to the rise in solar radiation. Specifically, the power output declined to 85.95 W when the solar radiation was $400\text{W}/\text{m}^2$, while it was 223.64 W when the solar radiation was $400\text{W}/\text{m}^2$.

It is important to note that the the characteristics I-V and P-V alter during the day in tandem with the increase in solar insolation. PVPs current, voltage, and output power rose as the solar radiation increased, while the temperature remained constant. The photovoltaic panel achieved its highest performance under standard test conditions (STC). The findings align with the research conducted by [1], [2], [6].

4. Conclusion

The performance evaluation of a PV module at different solar irradiance for power generation was carried out with Scilab Xcos™ simulation software with data under STC for Ilorin North Central, Nigeria. The block diagrams and equations for each of the PV modules' subsystems and components were examined. The simulation's findings demonstrate that when solar irradiation varies from $400\text{W}/\text{m}^2$ to $1000\text{W}/\text{m}^2$, there was a linear increase for both the V_{oc} and I_{sc} . This linear increase is caused by the amount of solar irradiance. Furthermore, the solar irradiation that the PV modules can capture determines output power of the PV modules. The quantity of irradiation the PV modules are able to extract directly relates to the output power of the PV module as seen in Figure 9, it also shows that the current and voltage reached their peak levels of 7.12 A and 15 V, respectively, when the solar radiation intensity was $1000\text{W}/\text{m}^2$. Their minimum values were 2.95 A and 14 V, respectively, when exposed to a solar radiation of $400\text{W}/\text{m}^2$. The power output of the photovoltaic (PV) panel grew in direct proportion to the rise in solar radiation. Specifically, the power output declined to 85.95 W when the solar radiation was $400\text{W}/\text{m}^2$, while it was 223.64 W when the solar radiation was $400\text{W}/\text{m}^2$.

The outcome of this study opens new avenues for designing a PV modules as well as PV arrays that would produce the highest possible power output at different solar irradiance which is the major problem faced by the particular geographical location chosen for this study.

Future research on the impact of dirt or shade on solar PV arrays as well as other algorithm setups for improved maximum power point tracking (MPPT) are suggested.

Author Contributions

Anas Bala: Conceived and designed the analysis, Methodology, Software, Validation, Analysis, Investigation, Data curation, Writing Original draft, Visualization, and Supervision.

Babatunde Moshood Alao: Methodology, Software, Validation, Analysis, Investigation, Data curation

Oyedun Aliu Olamide: Writing Original draft, Validation, Visualization, Supervision

Oluwaseyi Omotayo Alabi: Data curation, Writing Original draft, Visualization

Mohammed Adamu: Data curation, Writing Original draft, Visualization

References

- [1] Anas, B., Muhammad, J.Y., Ali, K.I., and Mshellia, R.B., Simulation of a PV module at different set-up and operating conditions to give IV and PV curves. *International Journal of Energy Studies*, 8(1), 1–13, 2023.
- [2] Al-Ghezi, M.K., Ahmed, R.T. and Chaichan M.T., The Influence of Temperature and Irradiance on Performance of the photovoltaic panel in the Middle of Iraq. *International Journal of Renewable Energy Development*, 11(2), 501, 2022.
- [3] Oufettoul, H., Lamdihine, N., Motahhir S., Lamrini, N., Abdelmoula, I.A. and Aniba, G., Comparative Performance Analysis of PV Module Positions in a Solar PV Array Under Partial Shading Conditions. *IEEE Access*, 11, 12176–12194, 2023.
- [4] Singh, H., Mathematical modeling of Solar photovoltaic system using Matlab/Simulink, 2022. Available online on:
http://136.232.12.194:8080/jspui/bitstream/123456789/499/1/1.%20front%20page%20harshit_Combine.pdf
- [5] Amalu, E.H. and Fabunmi, O.A., Thermal control of crystalline silicon photovoltaic (c-Si PV) module using Docosane phase change material (PCM) for improved performance. *Solar Energy*, 234, 203–221, 2022.
- [6] Amateur, A., Berrada, A., Loudiyi, K. and Aggour, M., Forecast modeling and performance assessment of solar PV systems. *Journal of cleaner production*, 267, 122167, 2020.
- [7] Etier, I., Nijmeh, S., Shdiefat, M. and Al-Obaidy, O., Experimentally evaluating electrical outputs of a PV-T system in Jordan. *International Journal of Power Electronics and Drive Systems*, 12(1), 421, 2021.
- [8] Chaudhary, A., *et al.*, Pomegranate peels waste hydrolyzate optimization by Response Surface Methodology for Bioethanol production. *Saudi Journal of Biological Sciences*, 28(9), 4867–4875, 2021.
- [9] Kouache, A.Z., Djafour, A. and Benzaoui, K.M.S., Performance analysis and effective modeling of a solar photovoltaic module based on field tests. *International Journal of Emerging Electric Power Systems*, 2024.
- [10] Suwapaet, N. and Boonla, P., The investigation of produced power output during high operating temperature occurrences of monocrystalline and amorphous photovoltaic modules. *Energy Procedia*, 52, 459–465, 2014.
- [11] Ike, C.U., The effect of temperature on the performance of a photovoltaic solar system in Eastern Nigeria. *Research Inventy: International Journal of Engineering and Science*, 3(12), 10–14, 2013.
- [12] Dash, P.K. and Gupta, N.C., Effect of temperature on power output from different commercially available photovoltaic modules. *International Journal of Engineering Research and Applications*, 5(1), 148–151, 2015.

- [13] Dubey, S., Sarvaiya, J.N. and Seshadri, B., Temperature dependent photovoltaic (PV) efficiency and its effect on PV production in the world—a review. *Energy procedia*, 33, 311–321, 2013.
- [14] Chander, S., Purohit, A., Sharma, A., Arvind, N.S.P., Dhaka, M.S., A study on photovoltaic parameters of monocrystalline silicon solar cell with cell temperature. *Energy Reports*, 1, 104-109, 2015.
- [15] Matter, K., El-Khozondar, H.J., El-Khozondar, R.J. and Suntio, T., Matlab/Simulink Modeling to study the effect of partially shaded condition on Photovoltaic array's Maximum Power Point. *International Research journal of engineering and Technology*, 2(02), 697–703, 2015.
- [16] Temaneh-Nyah, C. and Mukwekwe, L., An investigation on the effect of operating temperature on power output of the photovoltaic system at University of Namibia Faculty of Engineering and IT campus. *Third International Conference on Digital Information, Networking, and Wireless Communications (DINWC), IEEE*, 22–29, 2015.
- [17] Li, Z., Yang, J. and Dezfuli, P.A.N., Study on the influence of light intensity on the performance of solar cell. *International Journal of Photoenergy*, 1–10, 2021.
- [18] Al-Waeli, A.H., Chaichan, M.T., Sopian, K., Kazem, H.A., Mahood, H.B. and Khadom, A.A., Modeling and experimental validation of a PVT system using nanofluid coolant and nano-PCM. *Solar Energy*, 177, 178–191, 2019.
- [19] Mitsubishi Electric. Photovoltaic Modules. 2009, Available online at: <https://www.mitsubishi-pv.de/datasheets/tjga6-datasheet.pdf>
- [20] Rahim, N.A., Ping, H.W. and Selvaraj, J., Photovoltaic Module Modeling using Simulink/Matlab. *Procedia Environmental Sciences*, 17, 537-546, 2013.

The Effects of Animal Bone Ash on Asphalt Pavement Mixtures

Burak Ontas ^a, Julide Oner ^{b*}

^a Usak University, Graduate Education Institute, Civil Engineering Department, Usak, Turkey

^{b*} Usak University, Faculty of Engineering and Natural Sciences, Civil Engineering Department, Usak, Turkey

✉: burakontas27@gmail.com ^a, julide.oner@usak.edu.tr ^{b*} : 0000-0001-7775-2372 ^a, 0000-0003-3229-152X ^{b*}

Received: 28.03.2024, Revised: 16.05.2024, Accepted: 20.05.2024

Abstract

This study focuses on alternative raw material sources to meet the demand for sustainable construction materials. Particularly, it is suggested that waste materials, such as animal by-products, could provide a solution for enhancing the mechanical properties and durability of asphalt concrete. The research aims to improve the physical and mechanical properties of asphalt concrete by utilizing bone ash obtained from Category 3 animal by-products through a hydrolysis procedure. Experiments conducted showed that the addition of 5% bone ash ensured maximum stability when used in conjunction with different percentages of bitumen. Overall, some positive developments were observed in the physical and mechanical properties of asphalt concrete containing animal bone ash, possibly due to strengthening the bond between aggregate particles and bitumen material. This study highlights the potential of animal bone ash in improving the mechanical properties of asphalt concrete and recommends a 5% bone ash addition for optimum stability and durability. However, further research and field tests are needed to better understand the long-term effects of animal bone ash and its performance under different road conditions.

Keywords: Sustainable construction materials, Asphalt concrete, Mechanical properties, Animal bone ash, Stability.

1. Introductions

With the rapidly growing world economy and expanding population, the need for new roads is expanding day by day. To meet this increasing demand, asphalt is the globally preferred road superstructure type. Asphalt can be applied both hot and cold and can withstand a variety of weather conditions. Hot asphalt mixtures are mixtures in which bitumen is used at high temperatures and are generally recommended for use on roads with heavy traffic. Cold mixtures are mixtures that can be used at low temperatures and are used on roads where there is little traffic and maintenance. Today, 92% of freight transportation and 95% of passenger transportation takes place on highways. Thus, the traffic capacity of 20 years ago has increased at least 5 times, and the axle weight, which is the basis of superstructure projects, has increased from 8 tons to 13 tons. This situation has led to the deterioration of asphalt concrete in a shorter time than the expected service life. The concept of deterioration in asphalt concrete is defined as the degree to which the expected serviceability decreases as a result of traffic loads and environmental interactions at the end of the design life of a pavement structure, and it has been emphasized that the explanation of serviceability concept and a more detailed examination of the subject are necessary [1].

Furthermore, environmental issues and their solutions have been prioritized in research and



studies conducted in the transportation sector. In this regard, research and studies began in the late 1950s [2]. Since the mid-1990s, various techniques have been investigated to reduce the energy consumption involved in the production of hot mix asphalt, which is particularly renowned for its high mixing and compaction temperatures. In addition, the increase in living standards, social development, inadequacy of existing resources, and rising material and energy costs have prompted highway engineers to explore alternatives for constructing new roads and improving existing ones [3]. A satisfactory superstructure design should be durable, resistant to permanent deformation, cost-effective, and environmentally friendly.

Recently, there has been an increasing demand for an asphalt mixture capable of withstanding various external loads and minimizing cracking. The designed lifespan of infrastructures typically spans around 20 years, considering anticipated traffic loads. In determining the thickness of the superstructure, the repetition of axle loads is a significant factor, and an increase in the repetition of heavy axle loads decreases the service life of the road. Under these conditions, thicker superstructures and higher costs have been required to achieve the same service life [4]. For this reason, the superstructure that provides the best stability should exhibit resistance against deformation and formation of wheel tracks under traffic loads. Neither excessively high nor low stability is desirable. High stability leads to asphalt cracking, while low stability results in wheel track depressions in the asphalt. Therefore, the aim is to achieve maximum stability at the optimum asphalt percentage [5].

Thom and Elliott (2009) stated that with the high modulus of hardness of asphalt, it is possible to obtain a pavement that can withstand high traffic loads without cracking [6]. Previous researchers such as Zaumanis and Mallick (2014) have confirmed that the use of waste or by-product materials instead of coarse or fine aggregates and even filler materials provides a promising improvement in the mechanical properties and durability of asphalt concrete [7]. Yan et al. (2013) concluded that the filler material has a significant impact on the lifespan of asphalt mixtures due to its high influence on strength, as well as its ability to increase resistance to water penetration and improve asphalt viscosity. Therefore, as highlighted by Muniandy et al., the properties of filler materials are crucial in asphalt mixture design both physically and chemically [8]. Furthermore, recent increases in demand for construction materials, particularly in road construction, alongside the inadequacy of existing resources, have prompted a search for alternatives such as the utilization of waste materials.

In addition, in recent years, the amount of solid waste generated has increased worldwide due to the growing population, leading to the consumption of natural resources. Over the next five years, a significant increase in solid waste production is expected, which is anticipated to contribute to various environmental issues. From municipalities providing solid waste services in Turkey, it has been determined that a total of 25.28 million tons of solid waste was collected, with 12.75 million tons in the summer season and 12.53 million tons in the winter season in 2006. The use of waste materials in infrastructure can reduce the consumption of traditional highway materials and consequently decrease the extraction and processing costs of these materials. Some researchers suggest using by-product materials in replacing subbase layer materials to utilize more waste materials, while other studies oppose this view due to transportation costs and the evaluation of waste materials, advocating the significance of using these materials in asphalt applications [9]. Many researchers are interested in the use of waste materials instead of traditional materials in construction. Studies where waste materials are used in concrete or asphalt mixtures have generally shown improvements in the durability and mechanical properties of hardened construction materials.

Bindu et al. (2020) investigated the potential use of cashew nut shell (CNS) ash in asphalt mixtures. Various amounts of ash were used as a partial substitute for the fine sand component

in asphalt concrete. The Marshall test was employed to determine the mechanical properties of the mixtures. The findings indicate that cashew nut shell ash can be used in asphalt concrete instead of fine sand up to 15% [10].

On the other hand, Sung et al. (2008) focused on the use of recycled waste lime instead of filler in asphalt mixtures. The results of this study demonstrate a significant improvement in stripping resistance and permanent deformation resistance at high temperatures [11]. The effect of coal waste dust as a filler in hot mix asphalt was investigated by Modarres and Rahmanzadeh (2014). Compared to the reference mixture, asphalt samples containing coal waste ash resulted in better stability and flexibility modulus [12].

Al-Busaltan (2016) selected two filler materials, namely Silica Fume (SF) and Rice Husk Ash (RHA), for up to 30% filler substitution. The results showed that Hot Mix Asphalt (HMA) design with less than 15% SF or 27.5% RHA met the requirements of local specifications. [13]. Furthermore, Tahami et al. (2018) reported that asphalt mixtures containing rice husk ash (RHA) and palm kernel ash (PKA) fillers showed higher stability and stiffness modulus compared to the control mixture. Moreover, the utilization of biomass ash has increased the thermal stability of the mixtures and enhanced the adhesive strength between asphalt and aggregates, leading to an increase in rut resistance and fatigue life of Hot Mix Asphalt (HMA) mixtures [14].

Furthermore, Sharma et al. (2010) and Choi et al. (2014) have demonstrated that fly ash can be used as a filler material in asphalt mixtures instead of filler [15-16]. Choudhary et al. (2018) investigated the effect of seven different waste materials, including glass ash, limestone ash, red mud, rice husk ash, brick dust, carbide lime, and copper waste, on bituminous mixture [17]. Waste filler bitumen mixtures have been tested for a range of mechanical properties compared to cement filler bitumen mixtures, including strength and resistance to moisture, wheel tracking, and cracking. The results have shown that the properties of waste filler mixtures are satisfactory and superior to traditional fillers. Waste mineral products (marble, granite, and steel slag) have been proposed as alternatives to conventional filler materials by Tarbay et al. (2018) [18].

Additionally, rice husk ash has been investigated as a waste filler material in hot asphalt mixtures by Sargin et al. (2013) [19]. In the asphalt concrete mixture, four rates of limestone have been used as traditional fillers (4%, 5%, 6%, and 7%). According to the Marshall Stability test, the highest stability was achieved using 5% filler. Rice husk ash has been used as a substitute for limestone filler at rates of 25%, 50%, 75%, and 100%. From the results, it can be observed that a mixture containing 50% limestone filler and 50% rice husk ash exhibits the highest stability compared to other percentages and control samples.

As a result of the study in which granular polymers and waste plastics were used as additives in asphalt concrete, it was determined that asphalt concrete produced with polymer additives in different configurations and ratios was more durable than traditional concrete [20].

Studies conducted over the past three decades regarding the use of polymers as additives in asphalt concrete and the results of these studies have been summarized by Y. Yıldırım (2005) [21]. In the study conducted by Navarro et al. (2004) it was observed that the addition of ground rubber tires to asphalt concrete improved the temperature-dependent properties of the asphalt concrete [22]. On the other hand, in this study, which serves as an example of polymer enhancement, it has also been demonstrated that the addition of rubber has positive effects on the long-term aging properties of asphalt concrete [23]. There is diversity observed in the methods used for evaluating the results of research conducted on asphalt concrete incorporating waste tires. Ground rubber and polymers have been added to asphalt mixtures, and improvement studies using rubber have yielded positive results compared to normal asphalt

concrete in terms of permanent deformation, wheel tracking, and low-temperature cracking [24].

Improvement studies have been conducted regarding the incorporation of various thermoplastic polymers, namely SBS, SEBS, EVA, and EBA, into asphalt. At the conclusion of the study, it was observed that different polymers exhibited varied effects on asphalt properties, particularly enhancing storage stability, creep resistance, and temperature-dependent characteristics [25, 26].

The modernization and intensified management of livestock farms, which have experienced rapid development in recent years, have brought forth numerous challenges. Concurrently, the accumulation of waste, holding significant economic potential, has emerged as a pivotal environmental concern amidst the rising livestock population. Substantial quantities of animal bones, such as those from cattle, have been generated, occasionally leading to complications in waste disposal procedures. Considering that approximately 15% of beef carcasses and 16% of lamb carcasses contain bones, the average solid waste output from a beef slaughterhouse is estimated at 275 kg per tonne of total live weight slaughtered, equating to 27.5% of the animal's weight [27].

As stated by Muhammed et al. (2012), following the incineration process, animal bones primarily consist of approximately 80% calcium and magnesium, with approximately 10% carbon and other substances [28]. Ali et al. (2019) utilized traditional and dynamic rheometer test methods to investigate the effects of Portland cement and waste animal bone additions on the asphalt binder properties. Increases in the additive content resulted in decreased penetration, increased softening point, and increased flash point, indicating enhanced stiffness and resistance to wheel tracking. Consequently, animal bone ash may possess some pozzolanic properties in hot asphalt mixtures [29].

While bitumen constitutes 5-7% by weight and approximately 15% by volume of the asphalt mixture, its performance significantly influences the overall performance of the road throughout its service life [30]. Thus, enhancing the performance of flexible pavements is directly linked to the quality of the bitumen utilized in the mixture [31]. The performance of bitumen can be enhanced through the addition of certain percentages of additives, which may include various commercial, natural, artificial, and industrial substances. Although this initially raises the construction costs of flexible pavements, it ultimately yields economic benefits by reducing maintenance and repair expenses over the road's service life, provided that a high-quality application is achieved [32].

This study investigates the use of animal bone ash as an adjunct to conventional filler material in hot mix asphalt, aiming to evaluate its impact on asphalt pavement performance.

2. Test Methods

2.1. Marshall Stability Test

Utilizing standardized testing methods such as TS EN 3720/12697, AASHTO T 245, and ASTM D 1559, the Marshall test serves as a laboratory procedure employed to assess the technical properties of asphalt mixtures. Developed specifically for determining the durability and performance of asphalt mixes utilized in highway construction, the Marshall test evaluates the flow characteristics of the asphalt mixture at elevated temperatures, thus gauging the material's resistance to deformation under high temperatures. Accurate determination of asphalt

flow properties, subjected to factors such as vehicular traffic and intense solar radiation, enables more precise performance predictions. Additionally, the Marshall test measures the stability of the asphalt mixture, indicating how the material will behave under the influence of gravity and high temperatures. This parameter reflects the strength and load-bearing capacity of the mixture, with higher stability values suggesting greater strength and durability. The Marshall test aids engineers in determining the optimal mix design by assessing the performance of various asphalt mix compositions, allowing for the optimization of the mix's composition and properties to achieve the best performance under specific road, traffic, or climatic conditions. Integral to the quality control and assurance processes of asphalt manufacturers and construction firms, Marshall testing ensures the adherence of asphalt produced to specified standards, facilitating the use of materials that meet quality criteria for long-lasting and dependable infrastructure.

2.1.1 Marshall stability test procedure

In an oven set to 160°C, a pre-determined aggregate sample weighing 1150 grams is left for one day (24 hours), while the bitumen is allowed to rest for 2-3 hours. Throughout the experiment, the molds, mixing sticks, shovels, and aggregate containers to be used must be kept in the 160°C oven to prevent any heat loss during the test. After removing the aggregate mixture from the oven, it is transferred to a mixer bowl, and a well is formed in the center to pour the bitumen into. A specific amount of bitumen, determined as a percentage of the aggregate weight at 3.5%, 4%, 4.5%, 5%, 5.5%, 6%, and 6.5%, is poured onto the aggregate as per the predetermined proportions. For each specified amount of bitumen, a total of 21 (3x7) samples are prepared, with three samples per designated bitumen percentage. The aggregate and bitumen are mixed in the mixer for 1.5-2 minutes. During this process, the mixer bowl is placed on the mixer heating device to prevent a drop in the mixture's temperature. Similarly, to prevent heat loss, the mixer head should be kept in the oven and utilized during mixing. As the mixing process nears completion, molds are removed from the oven and greased with Vaseline or a similar substance to prevent sticking. Greased or impermeable paper cut to suitable sizes is placed at the bottom of the mold. The mixture is scooped from the mixer, poured into the mold, and compacted using a tamper. The temperature of the mixture is measured at this stage, and greased or impermeable paper is placed on top of the mixture again. The temperature of the mixture should not drop below 140°C at this point. The mold containing the sample is placed on a Marshall hammer, and 75 blows are applied to each side for Hot Mix Asphalt (HMA) or 50 blows for Stone Mastic Asphalt (SMA). Care should be taken during compaction to ensure that there is no material loss from the sample. The mold is then placed on a clean, flat surface to allow the sample to cool. The papers on the top and bottom surfaces of the sample should be removed before the sample cools to prevent them from sticking. The molds are left to cool for approximately 3 hours. After cooling, the samples are removed from the molds using a jack, labeled, and marked. The samples are left for one day at room temperature. The next day, if there are any protrusions around the samples, they are cleaned. Height measurements are taken from the samples using a caliper. Measurements should be taken from approximately 120°C apart at three different points on the sample. The weights of the samples in air and water are measured and recorded. The samples are left in a water bath at 60°C for 30 minutes. After being removed from the water bath, the samples are dried and placed in the Marshall strength device. The device is operated, applying a load to the sample at a speed of 51 mm/minute. As a result, flow and strength values of the sample are obtained. The results obtained from applying all the previous steps to all samples, including height, weight in air and water, Marshall flow and strength values, are arranged in table format. Flow and strength values for samples are multiplied by correction factors based on their heights and added to the table. The purpose of using Marshall correction factors is to ensure the evaluation of samples with different heights

under the same conditions. Three samples were prepared for each bitumen ratio, and the conformity of the results obtained from these samples is checked by plotting a "Bitumen Ratio (%)- Air Void (%)" graph. If the results on the graph are close to each other, it is accepted that the test results are consistent and compatible, and the calculations continue. Based on the results obtained from the prepared Marshall Table, "Bitumen ratio Practical specific gravity", "Bitumen ratio-Marshall strength", "Bitumen ratio-air void ratio", and "Bitumen ratio-Void filled with bitumen ratio" graphs are drawn. According to these graphs, the bitumen ratio corresponding to the maximum practical specific gravity value, the bitumen ratio corresponding to the maximum Marshall strength value, the bitumen ratio corresponding to the 4% air void ratio value (mean of lower and upper air void level for wearing course), and the bitumen ratio corresponding to the 70% void filled with bitumen ratio value are determined. The average of these four bitumen ratios is calculated to find the optimum bitumen ratio for the mixture. To determine whether the found optimum bitumen ratio falls within the specification limits, a "Bitumen Ratio-Flow" graph is plotted. The optimum bitumen ratio is accepted if it meets the flow limit.

2.2. Modified Lottman Test (AASHTO T-283)

One of the most important studies conducted to determine the usability of Hot Mix Asphalt (HMA) in road pavement is the measurement of the mixture's sensitivity to water. The AASHTO T-283 test is widely used to determine the sensitivity of compacted HMA to the effects of water. Developed by Lottman in the 1970s, the test conditions were modified and standardized by AASHTO. The test is aimed at determining the strength loss of the mixture due to water. The results obtained are used to determine the sensitivity of hot mixtures to stripping in long-term service processes on roads [33, 34, 35]. Compacted asphalt samples are divided into two groups: dry and conditioned (wet), and subjected to the indirect tensile test to determine the mixture's strength loss. The reason for obtaining the indirect tensile strength of the mixture is that it is one of the most important parameters for the continuity of hot mix wearing layers, as the tensile strength of the hot mix is critical for resisting the tensile stresses caused by traffic and environmental effects. If this strength is low, the mixture may deteriorate due to the tensile stresses generated by traffic and environmental factors. At the conclusion of the study, it was observed that different polymers exhibited varied effects on asphalt properties, particularly enhancing storage stability, creep resistance, and temperature-dependent characteristics [36]. For each test group to be subjected to the test, at least 6 samples are prepared, consisting of 3 unconditioned and 3 conditioned specimens. The prepared uncompacted mixture samples are placed in trays and cooled at room temperature for 2 hours, then placed in an oven at 60°C for 16 hours. The mixture samples, which are allowed to stand for 2 hours at the compaction temperature, are compacted at 6–8% air voids and left at room temperature for 24 hours. Dry specimens not subjected to conditioning are soaked in a water bath at 25°C for 2 hours and then subjected to the indirect tensile test to failure. For the conditioned specimens, a vacuum is applied with a manometer for 5–10 minutes at 13–67 kPa suction pressure to saturate them with 70–80% water content. The saturated specimens are placed in a freezer at -18°C for 16 hours. After removal from the freezer, the specimens are placed in a water bath at 60°C for 24 hours, then removed and placed in a water bath at 25°C for 2 hours before being subjected to the indirect tensile test. The ratio of the indirect tensile strength of the conditioned specimens (ITS_{wet}) to that of the unconditioned specimens (ITS_{dry}) is calculated using the following equation:

$$ITSR = (ITS_{WET}/ITS_{DRY}) \times 100 \quad (1)$$

ITSR Indirect tensile strength ratio (%),

ITS_{wet}: Average indirect tensile strength (kPa) of the conditioned (wet) group,

ITS_{dry}: Average indirect tensile strength (kPa) of the unconditioned (dry) group.

According to the Superpave mixture design method, for HMA to be deemed sufficiently resistant to water effects, the ITSR (Indirect Tensile Strength Ratio) value should be at least 80% [37, 38]. However, in the original Lottman method, it is considered sufficient for this value to be at least 70%. Hot mixtures with an ITSR value lower than 80% in the test are generally deemed to lack sufficient resistance to water effects, and measures are taken to enhance the mixture's water resistance. Typically, anti-stripping additives are added to increase the mixture's resistance to water effects. For modified mixtures using additives, the ITSR value is expected to be at least 85% [35, 37].

2.3 Materials

Typically, for hot asphalt mixtures, a composition of approximately 95% aggregate, 5% bitumen, and additives is used. In this study, filler and animal bone ash were utilized as aggregate, bitumen, and additive, respectively.

2.3.1 Bitumen

The bitumen used for this research was sourced from Compañía Española de Petróleos, S.A.U. The test results of the bitumen are indicated in Table 1.

2.3.2. Aggregates

The aggregate used in the research was supplied by CONTEC- Construções e Engenharia, S.A. The gradation values of the aggregate are shown in Fig. 1, while the physical properties of the aggregates and specification requirements are presented in Table 2.

Table 1. Bitumen test results

TESTS	UNIT	NORM	RESULTS	SPECIFICATIONS LIMITS	
				MIN	MAX
Penetration (25 °C; 100g; 5s)	0.1mm	EN 1426	39	35	50
Penetration index	-	EN12591	0,1	-1.5	0.7
Softening temperature	°C	EN1427	54	50	58
Fraass brittleness temperature	°C	EN12593	-1	-	-5
Resolution	%	EN 12592	130	99	-
Ignition temperature	°C	EN2592	280	240	-
Resistance to ageing at 163 °C (EN 12607-1)					
Mass change	%	EN 12607-1	0.2	-	0.5
Retained penetration (25 °C; 100g; 5s)	%	EN 1426	62	53	-

Table 2. Physical properties of aggregates and specification requirements

Property	Standard	Units	Gneiss 8/20	Gneiss 4/22	Sand 0/4	Filler	Limit
Flakiness index (FI)	EN 933-3 (34)	%	FI ₁₅	FI ₁₆	FI ₂₀
Resistance to fragmentation: Los angeles (LA)	EN 1097-2 (35)	%	LA ₂₀	LA ₂₁	LA ₃₀
Resistance to wear: micro-Deval (M ₀₈)	EN 1097-1 (36)	%	M ₀₈ 10	M ₀₈ 10	M ₀₈ 15
Polished stone value (PSV)	EN 1097-8 (37)	%	PSV ₃₀	PSV ₃₀	PSV ₃₀
Water absorption (WA)	EN 1097-6 (38)	%	0.5	0.6	0.6	WA ₂₄ 1
Assessment of fines: methylene blue (MBr)	EN 933-9(39)	g/kg	MBr10	MBr10	MBr10
Voids of dry compacted filler(V)	EN 1097-4 (40)	&	32	V _{24/34}
Delta ring and ball (°C)	EN 13179-1 (41)	°C	14

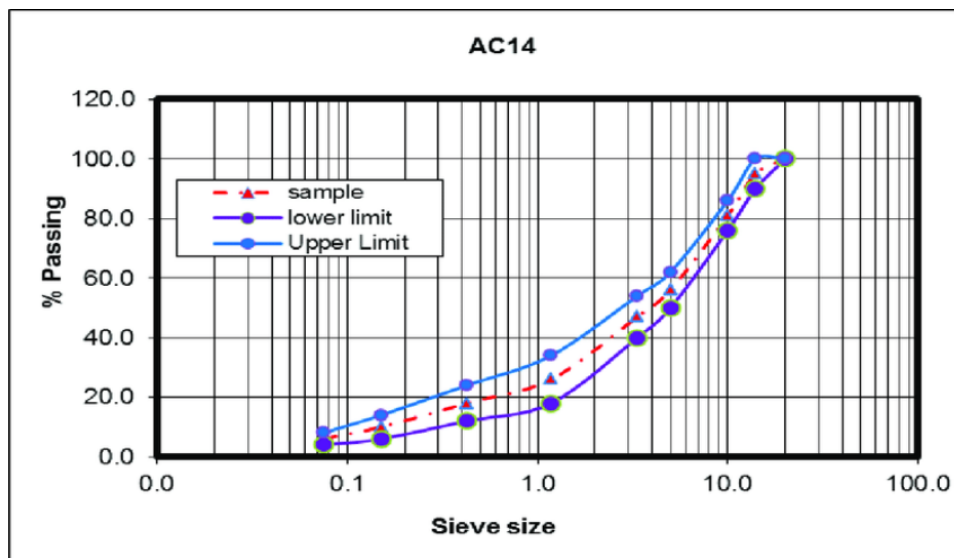


Fig. 1. Grading of the aggregate's mixture and specification limits

2.3.3 Animal bone

The bone used in the study was sourced from Sebol - Comércio e Indústria de Sebo, S.A. Bone meal is a product obtained from the hydrolysis procedure of Category 3 animal by-products selected in compliance with Regulation 1292/EC. This regulation dates back to August 5, 2005. Tri-calcium phosphate derived from animal bones is recognized as a feed product under Article 11.3.4 of Regulation (EC) No 2017/1017 dated June 15.

The hydrolysis procedure is the process whereby the chemical bonds of a substance are broken

or decomposed through the action of water. In this process, water molecules break the chemical bonds between the components, thereby breaking the molecules into smaller parts. The hydrolysis procedure in animal bones is predominantly a chemical process that occurs under specific temperature and pressure conditions. This process is typically conducted using a solution or reagent that acts as a hydrogen donor.

During this process, the organic components within the bones are decomposed by the action of water under high temperature and pressure. In this decomposition process, proteins can be converted into amino acids, fats into free fatty acids, and minerals into more soluble forms. Consequently, the product obtained as a result of hydrolysis becomes more digestible and easier to process.

The aim of the study is to investigate the changes in the mechanical and physical properties of the mixture with the use of animal bone ash. For this purpose, animal bone ash was used in each sample up to 5% of the bitumen content. The properties of bone meal are specified in Table 3.

Table 3. Physical and chemical properties of animal bone

FORM	Colour	Odor	Density
Ash	White to gray	Typical	0.80 Kg/m ³
CONSERVATION			PACKAGING
In cool and dry conditions			Big Bags (0.8 ton)
REFERENCE PARAMETERS			
DESGINATION	UNIT	VALUE	REFERENCE
Crude protein	%	±9	
Ash	%	±84	
Moisture	%	±3	
Calcium	%	±28	Internal quality criteria
Phosphorous	%	±14	
Ash insoluble in HCl	%	±1	
Phosphorous insoluble in citric acid 2%	%	±7	

3. Experimental Studies

3.1. Marshall Test Results

Marshall test results for Hot Mix Asphalt (HMA) mixtures containing 5% animal bone ash used in conjunction with bitumen are depicted in Fig. 2., 3., 4., 5., 6.,7. and 8., showing the volumetric specific gravity (D_p , g/cm³), maximum theoretical specific gravity (D_t , g/cm³), air voids (V_h , %), voids in mineral aggregates (VMA, %), voids filled with bitumen (VFA, %), stability, and flow values, respectively.

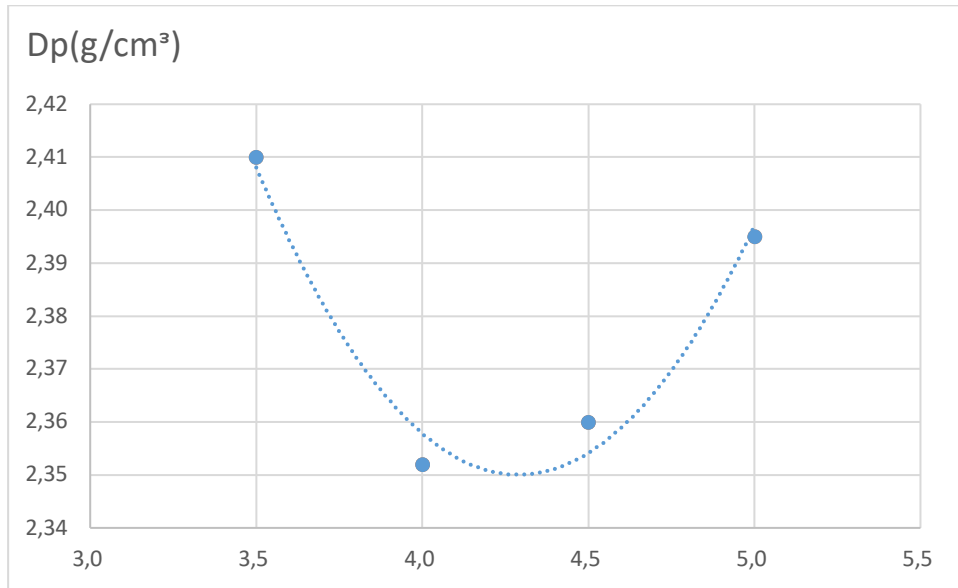


Fig. 2. Volume specific gravity

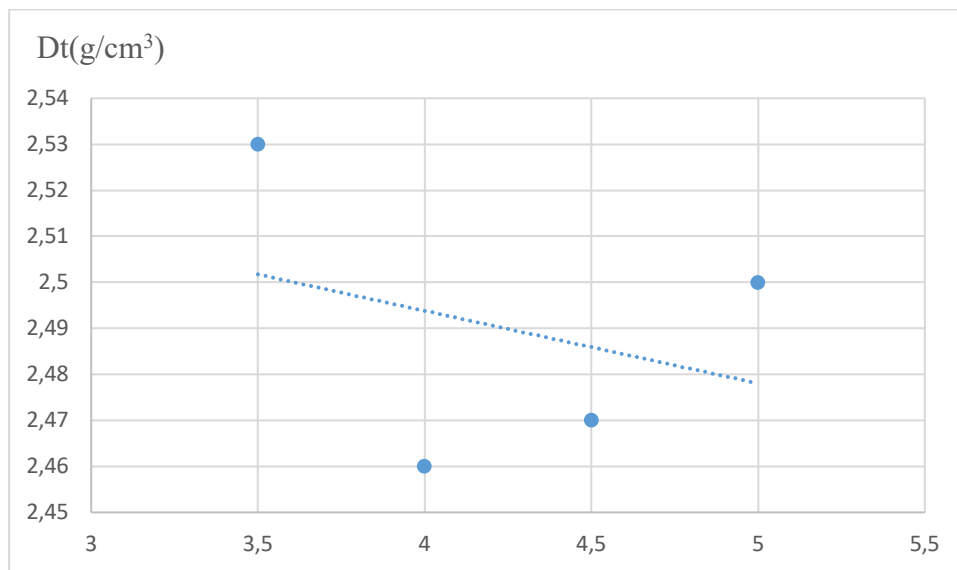


Fig. 3. Maximum theoretical specific gravity

As seen in Fig. 2. and 3., the volumetric specific gravity and maximum theoretical specific gravity values of hot mix asphalt samples prepared with four different percentages of bitumen and containing 5% animal bone ash exhibit a decrease from 4% to 3.5% bitumen addition, while an increase is observed at 4.5% and 5% bitumen additions.

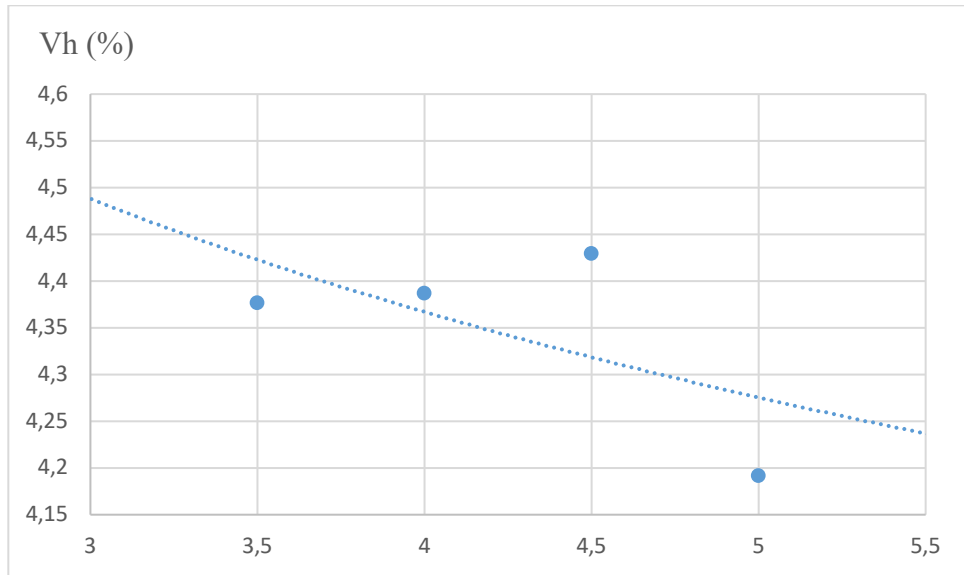


Fig. 4. Air void percentage

Fig. 4. shows that the highest air void content is observed at 4.5% bitumen addition, while the lowest air void content is observed at 5% bitumen addition. All prepared HMA samples remained within the specified limits of the KGM specification.

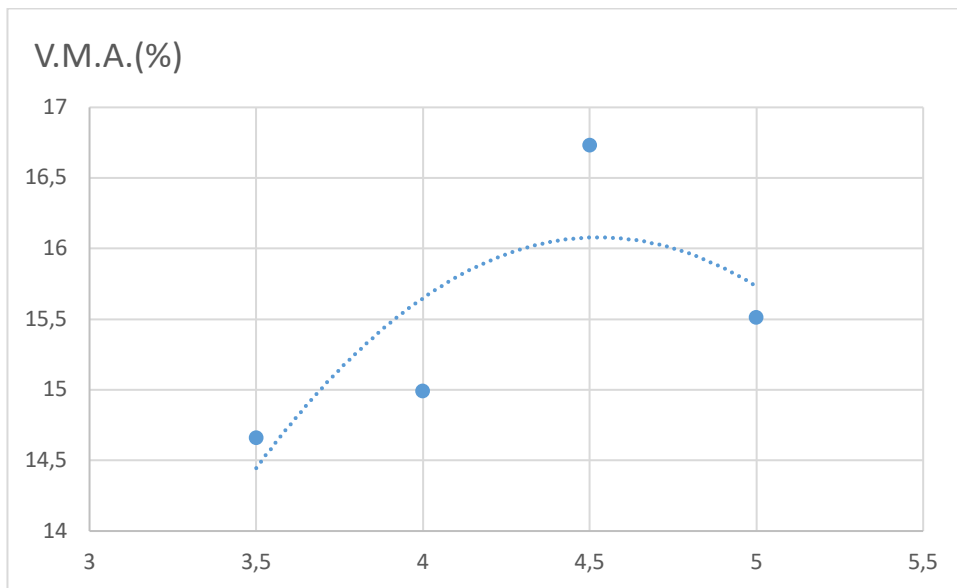


Fig. 5. Percentage of voids between aggregates

Fig. 5. indicates that the inter-aggregate void value increased compared to 3.5% bitumen addition at 4% bitumen addition, while it decreased compared to 4.5% and 5% bitumen additions. Each HMA mixture containing 5% animal bone ash remained above the minimum specified inter-aggregate void percentage in the KGM specification.

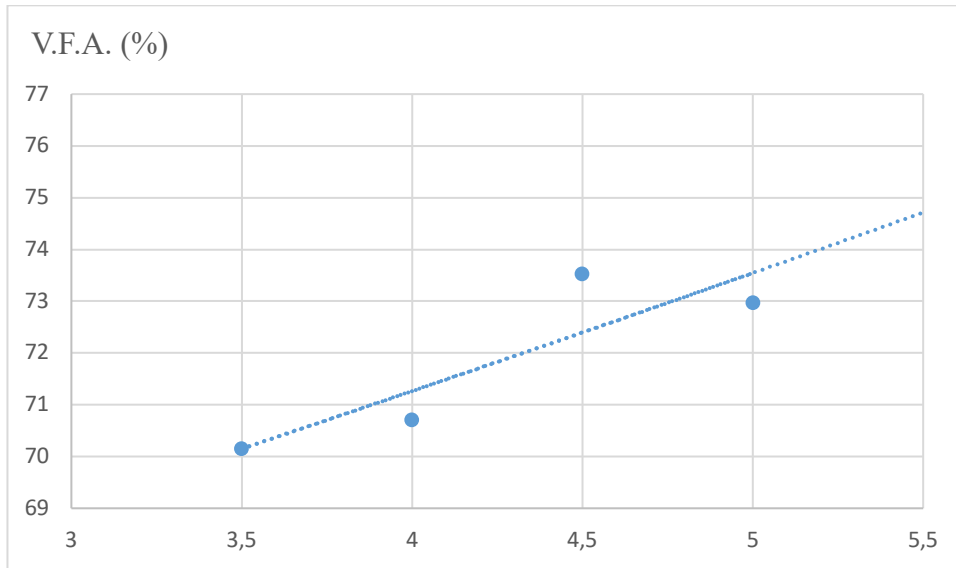


Fig. 6. Aggregate filled void percentage

Fig. 6. shows that the inter-aggregate filled void ratio has the highest percentage at 4.5% bitumen addition, while it has the lowest percentage at 3.5% bitumen addition. The HMA mixture prepared with 4% bitumen addition has a lower aggregate filled void ratio than the HMA mixture prepared with 5% bitumen addition. Each HMA mixture remained within the specified limit values in the KGM specification.

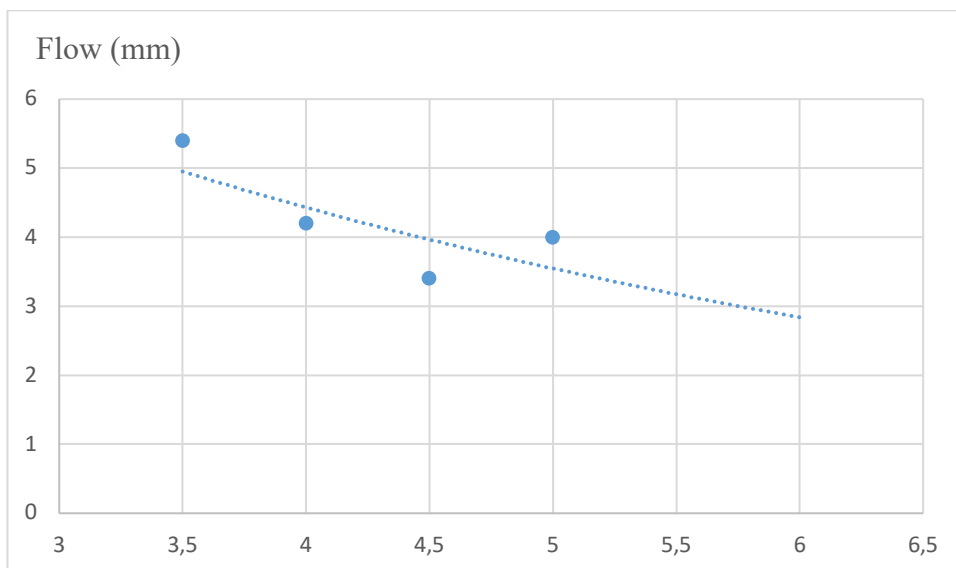


Fig. 7. Flow values

Fig. 7. indicates that the HMA mixture with a 3.5% bitumen content provides the highest flow value, while the HMA mixture with a 4.5% bitumen content provides the lowest flow value. It was observed that the addition of 4% bitumen results in a higher flow value compared to the addition of 5% bitumen. HMA mixtures with 4.5% and 5% bitumen content remained within the specified limits according to the KGM specification. The flow values of HMA mixtures with 3.5% and 4% bitumen content exceed the specified limit values in the specification.

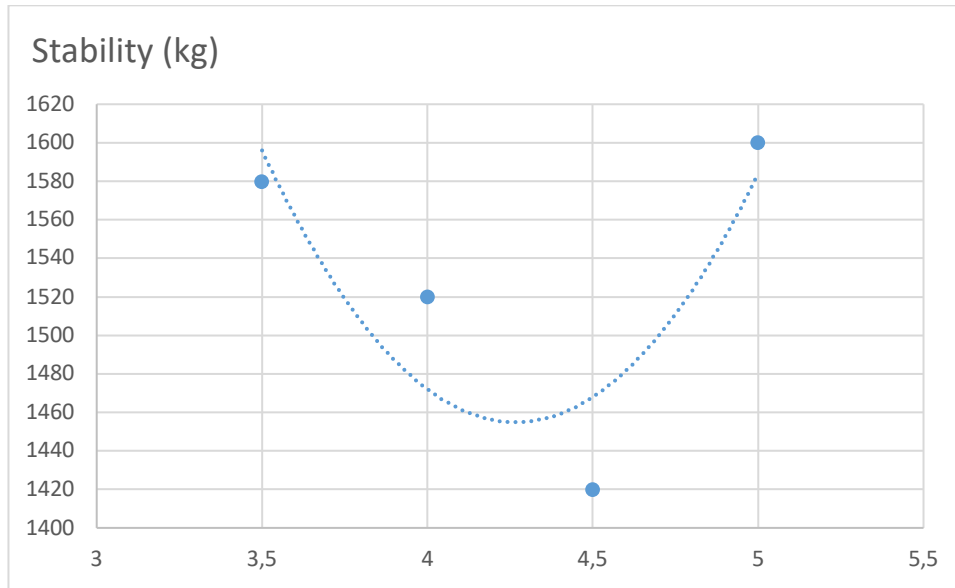


Fig. 8. Stability values

In Fig. 8., it is observed that the HMA mixture with a 4.5% bitumen content provides the lowest stability value, while the HMA mixture with a 5% bitumen content provides the highest stability value. The HMA mixture with a 4% bitumen content is lower compared to the HMA mixture with a 3.5% bitumen addition. Each HMA mixture prepared according to the KGM specification has exceeded the specified lower limit value.

The volumetric specific gravity (D_p) of the test specimens was determined by measuring the weight in air, weight in water, and saturated surface-dry weight for each HMA specimen removed at room temperature. After calculating the maximum theoretical specific gravity (D_t), the air void content (V_h), voids in mineral aggregates (VMA), and voids filled with bitumen (VFA) were determined, and the optimum bitumen content of the HMA mixtures was obtained from the graphs. Flow and stability results were obtained by conducting Marshall stability tests. The results obtained from the graphs are summarized in Table 4.

Table 4. Summarized Marshall test results

	3	4	4.5	5	Specification
Animal bone ash%	3	3	3	3
Bitumen %	3.5	4	4.5	5	4--7
D_p (g/cm ³)	2.419	2.352	2.361	2.395
D_t (g/cm ³)	2.53	2.46	2.47	2.5
V_h %	4.377	4.387	4.43	4.192	3--5
V.M.A. %	14.664	14.994	16.734	15.513	min. 14
VFA %	70.153	70.708	73.528	72.978	65--75
Flow (mm)	5.4	4.2	3.4	4	2--4
Stability (kg)	1580	1520	1420	1600	min. 900

As seen in Table 4, the air void content (V_h) of each HMA mixture specimen remains within the specified range of 3-5% according to the KGM specification. The voids in mineral

aggregates (VMA) are associated with the deformation resistance and durability of the asphalt mixture. According to the KGM specification, the VMA value should be a minimum of 14%. Each HMA specimen meets the minimum specification criterion.

According to the KGM specification, the voids filled with bitumen (VFA) in the asphalt should be between 65-75%. Each of the prepared HMA specimens falls within these limit values.

Marshall stability and flow tests were conducted according to TS EN 12697-34 standard. In the standard, stability is defined as the maximum resistance to deformation, and flow is defined as the deformation that occurs in the specimen when it reaches maximum load. According to the KGM specification, the minimum stability value is 900 kg, while the flow limit values range between 2-4 mm.

According to the test results, all specimens prepared with the addition of 5% animal bone meet the minimum stability value, using different bitumen percentages. When evaluating the flow values of specimens prepared with different bitumen percentages with the addition of animal bone together, it is determined that specimens containing 4.5% and 5% bitumen meet the specification limits.

3.2.2 Modified Lottman test results (AASHTO T-283)

For the experiment, an optimum bitumen-animal bone ash ratio of 5% was selected, and 3 unconditioned (dry) and 3 conditioned (wet) specimens were prepared in compliance with the specifications. As a result of the experiments, indirect tensile strength (ITS) values were determined.

ITS_R: Indirect tensile strength ratio (%), ITS_{wet}: Average indirect tensile strength of the conditioned (wet) group (kPa), ITS_{dry}: Ratio of average indirect tensile strength of the unconditioned (dry) group (kPa) were calculated. The results of the experiments are shown in Table 5., Table 6. and Table 7.

Table 5. Unconditioned sample Modified Lottman test (AASHTO T-283) results

SAMPLE TYPE	No	Unconditioned Samples		
		Height (mm)	P max (kN)	ITS dry (kPa)
B+%5 BA	5	62.8	23.53	2329
	6	62.4	29.75	2967
	7	62	26.01	2631
ITS _{dry} average=				2642.33

As seen in Table 5., the specimen prepared with a 5% bitumen content, specifically the B6 specimen with a height of 62.4 mm, exhibits the maximum load-carrying and tensile strength. The B5 specimen has the lowest tensile and load-carrying capacity, whereas the B7 specimen demonstrates greater tensile and load-carrying capacity compared to the B5 specimen.

Table 6. Conditioned sample Modified Lottman test (AASHTO T-283) results

SAMPLE TYPE	No	Conditioned Samples		
		Height (mm)	P max (kN)	ITS wet (kPa)
B+%5 BA	1	63.9	19.15	1868
	2	62.5	21.94	2191
	3	63.2	18.68	1843
ITS _{wet} average=				1967.33

As observed in Table 6., the specimen prepared with a 5% bitumen content, specifically the B2 specimen with a height of 62.5 mm, exhibits the maximum load-carrying and tensile strength. The B3 specimen has the lowest tensile and load-carrying capacity, while the B1 specimen demonstrates greater tensile and load-carrying capacity compared to the B3 specimen.

Table 7. ITSR value

ITSR (%)
ITS _{wet} /ITS _{dry} =0.74

The modified Lottman test was utilized to determine the resistance of the asphalt concrete mixture to water damage using the optimum bitumen content. Indirect tensile strength tests were conducted on conditioned and unconditioned identical specimens of the HMA mixture. Three samples were used for each option, and the average of the values obtained from the three samples was considered. The ITSR value was determined by comparing the ITS values of conditioned and unconditioned specimens. The calculations are summarized in Table 5. According to the KGM specification, the minimum ITSR value should be 0.80, but the conducted experiment did not meet this requirement. The ITSR value obtained from the experiment was 0.74, indicating that the sample has low tensile strength and is prone to cracking and deformation.

5. Conclusion and Recommendations

This study aims to explore a more economical and beneficial way to recycle animal bones, a type of environmental waste, for use in asphalt pavement. Previous research suggests that animal bone ash can increase the tensile strength and improve the flexibility of asphalt mixtures. Furthermore, the use of recycled materials can reduce costs, contribute to the reduction of environmental waste, and help us use resources more efficiently.

From the findings of this study, it can be concluded that the stability value of each HMA mixture remains above the minimum specified limit in the relevant specifications, which could be attributed to the finer particles of animal bone ash having a larger surface area, thus enhancing the asphalt and improving deformation resistance. Building upon previous studies, the higher percentage of calcium in bone ash promotes better bonding, contributing to the improvement of mechanical properties of asphalt.

HMA mixtures prepared with 4.5% and 5% bitumen content did not meet the flow limit values

and were not compliant with the specifications. This may be due to the proportion of animal bone ash, as the decrease in bitumen percentage also reduces the proportion of animal bone ash in the mixture. The decrease in the percentage of animal bone ash leads to increased air voids between aggregates, resulting in decreased stability and increased flow, as well as a decrease in the voids filled with asphalt.

Experimental findings confirm this situation. It is known that the highest animal bone content is in the 5% bitumen sample, and the lowest animal bone ash content is in the 3.5% bitumen sample. According to the test results, the highest stability value is observed with 5% bitumen addition, while the highest flow value is observed with 3.5% bitumen addition.

The sample with 5% bitumen addition was selected as the optimum bitumen, and the modified Lottman test was performed based on these sample ratios.

According to the experimental findings, the indirect tensile strength ratio (ITSR) being 0.74 indicates that the asphalt mixture does not meet the standard requirements for tensile strength and elastic properties. The fact that it does not meet the minimum requirement of 0.80 specified by the relevant authority suggests that the mixture may be more susceptible to cracking and deformation. Therefore, the use of bone ash may have adverse effects on tensile strength (ITS) and maximum load capacity (Pmax). However, in the original Lottman test, an ITSR value of at least 0.70 is considered sufficient.

Using HMA mixtures in asphalt reduces the use of traditional highway materials, thus reducing costs and helping to reduce the environmental damage caused by waste materials.

Acknowledgments

This study was conducted with the support and resources provided by Instituto Superior de Engenharia de Coimbra.

Author Contributions

Burak Ontas: Conceived and designed the analysis, Performed the analysis, Wrote the paper, Modified the paper.

Julide Oner: Conceived and designed the analysis, Contributed data and analysis tools, Performed the analysis, Wrote the paper.

References

- [1] Dağdelen, E., *Investigation of the Effect of Heat on the Physical Properties of Asphalt Concrete*, Firat University Institute of Science; Master's Thesis, 1995.
- [2] Al-Hadidy, A.I., Tan, Y.Q., Mechanistic analysis of ST and SBS-modified flexible pavements. *Construction and Building Materials*, 23(8), 2941-2950, 2009.
- [3] Şengöz, B., Topal, A., Use of asphalt roofing shingle waste in HMA. *Construction and Building Materials*, 19(5), 337-346, 2005.
- [4] Polat, H., *Analysis of the Physical Properties and Compaction of Bituminous Mixture Surface Layers of Ankara Gerede, Ankara Ring Road*, Gazi University Institute of Science, 1994.

- [5] TS 118: Petroleum products, determination of needle penetration of bitumens and bituminous binders, *Turkish Standards Institution*, 1998.
- [6] Thom, N., Elliott, R., *Asphalt properties and test methods: In ICE Manual of Construction Materials*, Fundamentals and Theory; 1st edition, 2009.
- [7] Zaumanis, M., Mallick, R. B., Examining the use of very high content reclaimed asphalt in plant-produced asphalt mixtures. *International Journal of Pavement Engineering*, 15(1), 39–55, 2014.
- [8] Yan, K. Z., Xu, H. B., Zhang, H. L., Effect of mineral filler on properties of warm asphalt mastics containing Sasobit. *Construction and Building Materials*, 48, 622–627, 2013.
- [9] Huang, Y., Bird, R. N., Heidrich, O., A review of the use of recycled solid waste materials in asphalt pavements. *Resources, Conservation and Recycling*, 52(1), 58–73, 2007
- [10] Bindu, C. S., Joseph, M. S., Sibinesh, P. S., George, S., Sivan, S., Evaluation of warm mix asphalt performance using natural rubber modified bitumen and cashew nut shell liquid. *International Journal of Pavement Research and Technology*, 13(4), 442–453, 2020.
- [11] Sung D., Hwang., Park H.M., & Rhee S.K., An Investigation on the Engineering Properties of Asphalt Concretes with Recycled Lime Filler. *Waste Management*, 28(1), 191–199, 2008.
- [12] Modarres, A., Rahmanzadeh, M., Application of waste coal ash in hot mix asphalt as filler. *Construction and Building Materials*, 66, 476–483, 2014.
- [13] El-Busaltan, Ş., Evaluation of Asphalt Mixtures Containing Waste and By-Product Material Fillers. *Kerbela University Journal*, (2), 130-141, 2016.
- [14] Tahami, S. A., Arabani, M., & Mirhosseini, A. F., Use of two biomass ashes as filler in hot mix asphalt. *Construction and Building Materials*, 170, 547–556, 2018.
- [15] Sharma, V., Chandra, S., Choudhary, R., Characterization of fly ash-bitumen modified mixes. *Construction and Building Materials*, 24(12), 2354–2360, 2010.
- [16] Choi, M. J., Kim, Y. J., Kim, H. J., Lee, J. J., Performance evaluation of rubber-derived fuel fly ash as mineral filler in hot mix asphalt. *Journal of Traffic and Transportation Engineering*, 7(2), 249–258, 2020.
- [17] Choudhary, J., Kumar, B., Gupta, A., Application of waste materials as filler in bituminous mixes. *Waste Management*, 78, 417–425, 2018.
- [18] Tarbay, E. W., Azam, A. M., El-Badawy, S. M., Asphalt mixtures with waste materials and by-products as mineral fillers. *Innovative Infrastructure Solutions*, 4(1), 1–13, 2018.
- [19] Sargın, Ş., Saltan, M., Morova, N., Serin, S., Terzi, S., Evaluation of rice husk ash as filler in hot mix asphalt concrete. *Construction and Building Materials*, 48, 390–397, 2013.
- [20] Yüceer, A., Çelik, O. N., The use of polymers in asphalt concrete and evaluation of waste plastics. *Chamber of Civil Engineers Journal*, 227-234, 1991.
- [21] Yıldırım, Y., Polymer modified asphalt binders. *Construction and Building Materials*, 21, 66-72, 2005.
- [22] Navarro, F. J., Partal, P., Martinez-Boza, F., Gallegos, C., Valencia, C., Thermo-rheological behaviour and storage stability of ground tire rubber-modified bitumens. *Fuel*, 83(14), 2041–2049, 2004.
- [23] Ruan, Y., Davison, R. R., Glover, C. J., The effect of long-term oxidation on the rheological properties of polymer modified asphalts. *Fuel*, 82(15–17), 1763–1773, 2003.

- [24] Navarro, F. J., Partal, P., Martinez-Boza, F., Valencia, C., Gallegos, C., Rheological characteristics of ground tire rubber-modified bitumens. *Chemical Engineering Journal*, 89(1–3), 53–61, 2002.
- [25] Lu, X., & Isacsson, U., Modification of road bitumens with thermoplastic polymers. *Polymer Testing*, 20(1), 77–86, 2001.
- [26] Isacsson, U., Lu, X., Characterization of bitumens modified with SEBS, EVA and EBA polymers. *Journal of Materials Science*, 34(16), 3737–3745, 1999.
- [27] Raza, H., Rizvi, Khattak, M. J., Gallo, A. A., Rheological and mechanistic properties of bone adhesive-modified asphalt binders. *Construction and Building Materials*, 88, 64–73, 2015.
- [28] Muhammed, A., Aboje, A. A., Auta, M., Cibril, M., Comparative analysis and characterization of bone adhesive as adsorbent. *Pelagia Research Library Advances in Applied Science Research*, 3(5), 3089–3096, 2012.
- [29] Asif, A., Ahmed, N., Adeel, M., Zaidi, S. B. A., Jameel, M. S., Qureshi, F. A., Asif, S. A., Performance evaluation of bone glue modified asphalt. *Advances in Materials Science and Engineering*, 3157152, 2019.
- [30] Ahmedzade, P., The investigation and comparison effects of SBS and SBS with new reactive terpolymer on the rheological properties of bitumen. *Construction and Building Materials*, 38, 285–291, 2013.
- [31] Gökalp, İ., Uz, V. E., Investigation of the Effect of Waste Vegetable Cooking Oils on the Properties of Pure Bitumen. *Journal of Engineering Sciences and Design*, 6(4), 570–578, 2018.
- [32] Gökalp, İ., Uz, V. E., Utilizing of Waste Vegetable Cooking Oil in Bitumen: Zero Tolerance Aging Approach. *Construction and Building Materials*, 227, 116695, 2019.
- [33] Bagampadde, U., *Investigations on Moisture Damage-related Behaviour of Bituminous Materials*. Civil and Architectural Engineering; Doctoral Thesis, 2005.
- [34] Hunter, E. R., *Evaluating Moisture Susceptibility of Asphalt Mixes*. University of Wyoming; Laramie, 2001.
- [35] Zaniwski, J., Viswanathan, A. G., *Investigation of Moisture Sensitivity of Hot Mix Asphalt Concrete*, West Virginia University, 2006.
- [36] Balta, İ., *Sensitivity of Bituminous Hot Mixtures to Moisture-Induced Deterioration*. Dokuz Eylül University Institute of Science, Izmir; Master's Thesis, 2004.
- [37] Lavin, P.G., *Asphalt Pavements*, Spon Press, London and New York, 444p, 2003.
- [38] The Asphalt Institute: *Superpave Mix Design*, Superpave Series No. 2 (SP-2), U.S.A, 1996.



Determination of Ship Length and Draft on the Planning Stage of Cruise Ports in Türkiye

Alp Küçükosmanoğlu

Burdur Mehmet Akif Ersoy University, Faculty of Engineering and Architecture, Department of Civil Engineering, Burdur, Türkiye

✉: akucukosmanoglu@mehmetakif.edu.tr, : 0000-0002-7551-1513

Received: 12.04.2024, Revised: 27.05.2024, Accepted: 12.06.2024

Abstract

The evolution of cruise tourism, despite facing unprecedented challenges from the Covid-19 pandemic, has shown resilience, with a rapid recovery observed in 2022. This manuscript emphasizes the significance of analyzing cruise ship length and draft data for Turkish ports to facilitate effective development planning. Despite data availability challenges, percentiles of ship lengths and drafts have been established, offering insights into port capacity and future infrastructure requirements. The examination of ship length and draft requirements highlights the diverse needs of ports from Alanya to Trabzon. Continuous monitoring and adjustment of development plans are essential to adapt to evolving industry trends, such as the increasing size of cruise ships. Projections indicate a consistent upward trend in ship sizes, emphasizing the need for forward-looking investment strategies. This study provides a foundation for informed decision-making in port development, offering insights to optimize port efficiency and competitiveness. By assessing regional effects and proposing pragmatic investment approaches, the manuscript serves as a valuable resource for guiding future infrastructure investments in Türkiye's maritime industry, ensuring its sustainable growth and competitiveness.

Keywords: Cruise Port, Ship Length, Ship Draft, Development Plan, Infrastructure Investment.

1. Introduction

Cruise tourism in the world started towards the end of the 1960s. The establishment of the world's cruise companies, such as NCL (Norwegian Cruise Line-1966), RCI (Royal Caribbean International-1968) and CCL (Carnival Cruise Lines-1972) coincided with these dates [1]. Cruise tourism is a type of tourism that allows passengers to accommodate, eat, drink, have fun, do activities and visit more than one settlement at the same sea travel.

Approximately 30 million people traveled by cruise, in 2019. The yearly change in total cruise tourism passengers in the world has been compiled between the years 2003 and 2022 [2 - 9]. There is a significant decrease in number of passengers in the cruise industry in 2020 and 2021 due to the Covid-19 pandemic (Fig. 1), while the total number of passengers increased by approximately 1,000,000 (~7%) passengers each year before the pandemic.

The coefficient of determination is 0.98 in the linear regression line for the total number of cruise passengers between the years 2003 and 2019, when the Covid-19 pandemic is not taken into account. This shows that the total number of cruise passengers between 2003 and 2019 is consistent with the linear regression line (shown in the dashed red line in the Fig. 1). The number of passengers, which decreased due to the Covid-19 pandemic, shows a rapid recovery in 2022. It is expected that the increase in passenger numbers will continue and the number of



passengers will exceed 30 million in 2023. It is also expected that the number of passengers will converge estimated linear regression line over time.

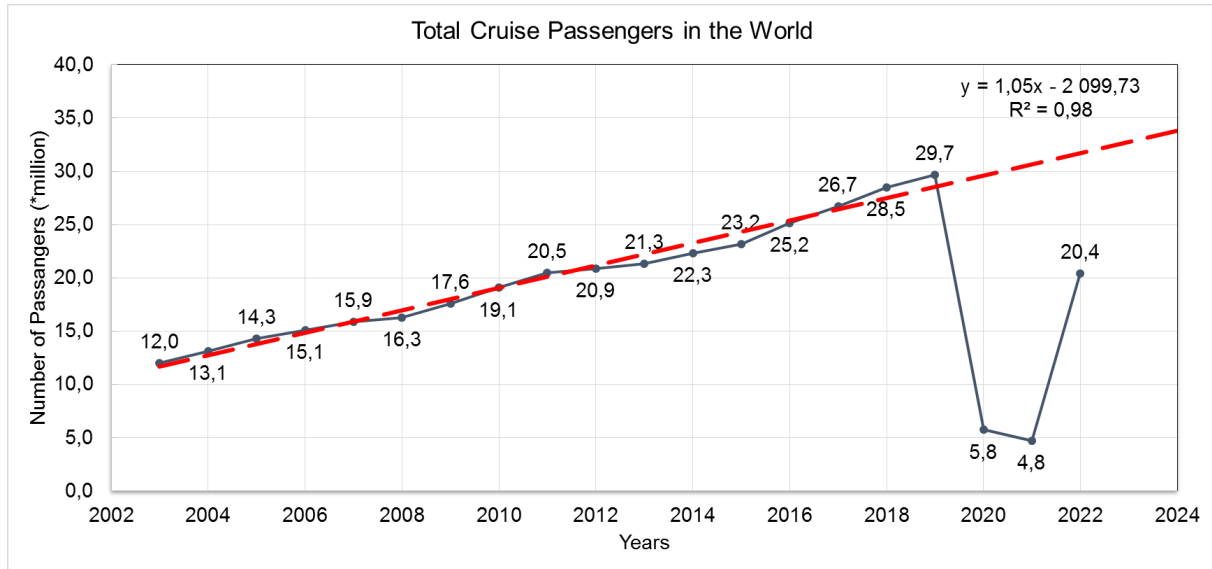


Fig. 1. Total cruise tourism passengers in the world

Cruise tourism in the world is organized in many regions. The most preferred regions are the Caribbean-Bahamas-Bermuda, Central and Western Mediterranean, Northern Europe, North America West Coast, Eastern Mediterranean, Asia and China, ...etc. in 2022. Approximately 1,13 million passengers (~5.6%) traveled to the Eastern Mediterranean and ~2,6 million passengers (~12.9%) traveled to Central and Western Mediterranean [10] out of a total of ~20,4 million passengers in the world.

Türkiye's cruise ports are mostly located in the eastern Mediterranean region. It is seen that the highest number of ships was 1,615 in 2011 and the highest number of passengers was 2,256,053 in 2013 (Table 1), when the number of ships and passengers arriving at Turkish ports between 2003 and 2023 [11, 12] is analyzed.

There is a decrease in the total number of ships from 2016 to 2022, due to the construction of the Galataport project between 2016 and 2021 and the Covid-19 pandemic. It is seen that Istanbul, which is an important center of attraction, has also negatively affected other cruise ports in Türkiye in this duration. However, it is estimated that the number of cruise ships and passengers visiting Turkish ports will continue to increase in the coming years, in parallel with the increase in the number of cruise passengers in the world.

The length and draft information of the cruise ships that will be served in the ports of Türkiye in the coming years is important in order to make development planning. Therefore, the length and draft of cruise ships arriving at Turkish ports have been compiled and analyzed. Thus, it is aimed to estimate the length and draft of cruise ships to be served in existing and planning ports.

Table 1. Total number of cruise ships and passengers arriving at Turkish ports

Years	Number of Ships	Number of Passengers
2003	887	581,840
2004	927	645,264
2005	1,048	757,563
2006	1,317	1,016,314
2007	1,421	1,368,400
2008	1,612	1,605,372
2009	1,328	1,484,194
2010	1,368	1,719,098
2011	1,615	2,190,098
2012	1,541	2,098,381
2013	1,530	2,259,053
2014	1,401	1,792,298
2015	1,440	1,888,522
2016	578	626,840
2017	307	306,485
2018	247	213,771
2019	344	300,896
2020	5	1,824
2021	78	45,362
2022	993	1,010,767
2023	1,192	1,542,522

The ship length and draft are significant parameters that will affect the amount of investment in the planning of a cruise port. The appropriate selection of the ship length and draft influences the payback period of the investment over the economic life of the cruise port. Selecting values larger than necessary will increase the amount of investment, while selecting values smaller than necessary will result in the inability to service the ships. In this study, it was intended to provide ideas and guidance for the existing and planned cruise ports in Turkey.

The data used in the research were verified by checking the IMO numbers of the ships. The data are compiled according to the schedules of cruise ships arriving at the ports of Türkiye. The results of the study can be validated by comparing them with the values that will be realized in the following years. Evaluations can be made based on the differences between the estimates and the actual values.

2. Material and Method

Data on cruise ship arrivals at Turkish cruise ports have not been archived regularly in the past. The arrival and departure dates and the ship name of the cruise ships coming to Alanya, Antalya, Bodrum, Çanakkale, Çeşme, Dikili, İstanbul, İzmir, Kuşadası, Marmaris and Trabzon ports can be compiled between 2020 and 2024 [13]. The name of the cruise ships arriving at the studied ports were checked with the International Maritime Organization (IMO) number and after that the ship length and draft were obtained. Tables containing information on ship name, IMO number, passenger capacity, ship length and ship draft were prepared for each port. It was found that a total of 145 different ships arrived at the ports studied in Türkiye.

Prepared ship length and draft data were examined to check the fitness of the normal distribution for each port. As a result of the examination, it was seen that the ship length and ship draft values did not fit the normal distribution. Therefore, a suitable distribution was searched but no suitable distribution can be found. The objective is to determine the ship length and draft for planning the development of a port. Therefore, percentiles of ship lengths (Table

2) and ship drafts (Table 3) were prepared for the studied ports and Türkiye (the total ships of the studied ports). The ship length and draft values were calculated at the 10th, 20th, 30th, 40th, 50th, 60th, 70th, 80th, 90th, 95th, and 99th percentiles for the studied ports and Türkiye. For example, the 10th percentile of the ship length and draft is determined by estimating that only 10% of the ships arriving at the port are serviced. Thus, the length and draft of the ships have been obtained for these percentage values.

Upon closer examination of the ship lengths obtained from our study, it becomes evident that different ports have varying requirements to accommodate incoming ships at different percentile levels. For instance, at Alanya port, ship lengths of 264 meters, 294 meters, and approximately 295 meters correspond to accommodating 90%, 95%, and 99% of incoming ships, respectively (Table 2). Similarly, in Antalya port, ship lengths of 295 meters, approximately 296 meters, and 316 meters cater to the same percentile levels of accommodated ships. This pattern extends across other ports such as Bodrum, Çanakkale, Çeşme, Dikili, İstanbul, Kuşadası, Marmaris, Trabzon, and throughout Türkiye. Each port has its specific requirements, reflecting its unique characteristics and capacities. These findings underscore the importance of tailoring development plans to meet the diverse needs of each port, ensuring efficient and effective accommodation of cruise ships now and in the future.

Table 2. Percentiles of ship lengths (m) served in the studied ports and for all vessels in Turkish ports

Percentiles (%)	Alanya	Antalya	Bodrum	Çanakkale	Çeşme	Dikili
10	181.00	105.00	110.50	134.00	181.00	111.00
20	204.00	181.00	160.00	159.00	200.00	112.00
30	207.00	206.50	199.00	160.00	206.60	112.00
40	207.00	210.17	210.17	181.00	210.17	112.00
50	207.00	211.00	224.00	181.00	210.17	159.00
60	214.65	237.20	244.00	228.00	210.17	181.00
70	226.64	242.00	268.00	228.00	210.17	206.50
80	241.60	253.33	277.00	228.00	210.17	211.00
90	264.00	295.00	294.00	229.00	210.17	217.20
95	294.00	295.26	295.00	229.00	211.00	224.00
99	294.28	316.00	315.24	237.58	230.61	230.58
Percentiles (%)	İstanbul	İzmir	Kuşadası	Marmaris	Trabzon	Türkiye
10	159.00	181.00	134.00	181.00	162.01	134.00
20	181.00	207.00	159.00	207.00	186.78	160.00
30	206.70	216.00	186.00	207.00	204.70	200.00
40	219.00	238.00	215.00	210.17	209.60	210.17
50	238.00	247.50	215.00	236.31	211.00	215.00
60	249.00	293.00	228.60	264.00	211.00	230.61
70	293.00	324.00	285.08	264.00	211.00	264.00
80	294.00	333.00	294.00	264.00	222.77	294.00
90	330.00	333.00	295.00	264.00	232.23	295.26
95	333.00	333.00	318.20	295.00	234.11	330.00
99	339.24	333.00	347.00	296.05	235.62	340.00

Upon scrutinizing the ship drafts obtained through our meticulous study, it becomes conspicuously clear that a spectrum of draft depths is imperative to adequately harbor incoming vessels at various percentile levels. In the bustling port of Alanya, for instance, ship drafts measuring 8.00 meters, 8.61 meters, and 8.90 meters are requisite to accommodate 90%, 95%, and 99% of incoming ships, respectively (Table 3). Similarly, in the bustling Antalya port, the requisite ship drafts are 8.20 meters, 8.25 meters, and 8.26 meters to cater to the same percentile levels of accommodated ships. This trend extends seamlessly across other critical ports such as Bodrum, Çanakkale, Çeşme, Dikili, İstanbul, Kuşadası, Marmaris, Trabzon, and encompasses the entirety of Türkiye's maritime infrastructure. Each port exhibits distinct draft depth exigencies, mirroring its idiosyncratic characteristics and capacities. These discernments underscore the paramount importance of tailoring development strategies to meet the multifaceted needs of each port, thereby ensuring the seamless and efficient accommodation of cruise ships both in the present and as we chart our course into the future.

Table 3. Percentiles of ship drafts (m) served in the studied ports and for all vessels in Turkish ports

Percentiles (%)	Alanya	Antalya	Bodrum	Çanakkale	Çeşme	Dikili
10	6.00	4.30	4.90	4.30	5.95	5.80
20	6.20	6.00	6.00	5.50	6.20	6.00
30	6.20	6.32	6.00	5.95	6.60	6.00
40	6.20	6.80	6.80	5.95	6.80	6.00
50	7.20	7.13	7.00	6.00	6.80	6.00
60	7.50	7.30	7.20	6.70	6.80	6.56
70	7.70	7.60	7.75	6.70	6.80	6.71
80	7.80	7.70	8.00	6.70	6.80	7.05
90	8.00	8.20	8.20	6.80	6.80	7.41
95	8.61	8.25	8.38	6.80	7.21	7.54
99	8.90	8.26	8.60	7.96	7.80	7.75
Percentiles (%)	İstanbul	İzmir	Kuşadası	Marmaris	Trabzon	Türkiye
10	5.95	6.20	5.50	6.00	5.46	5.80
20	6.00	6.80	6.00	6.20	6.11	6.00
30	6.70	7.20	6.20	6.37	6.60	6.20
40	7.05	7.50	6.80	6.80	6.60	6.80
50	7.60	7.70	6.80	7.30	6.60	6.80
60	7.80	8.14	7.50	8.00	6.73	7.50
70	8.10	8.60	7.85	8.00	7.19	7.80
80	8.30	8.65	8.00	8.00	7.46	8.00
90	8.60	8.65	8.60	8.00	7.66	8.60
95	8.70	8.65	8.70	8.20	7.73	8.65
99	9.00	8.65	9.10	8.22	7.79	8.90

The size of a ship arriving at a port is influenced not only by the facilities provided by the port but also by the characteristics of the destination. Some ports receive large cruise ships while others receive smaller cruise ships. Thus, the study was able to assess the regional effect on ship length and ship draft. In addition, the size of ships has also been increasing over the years. The change in ship length and ship draft values over time has been compiled depending on the year of construction of the ships arriving at Turkish ports. It is estimated that the ship length will reach 400 meters in approximately 2050 according to the linear regression curve fitted

between ship length and year of construction (Fig. 2). An annual increase of 2 meters in ship length is expected considering the ship length increase by 50 meters in about 25 years.

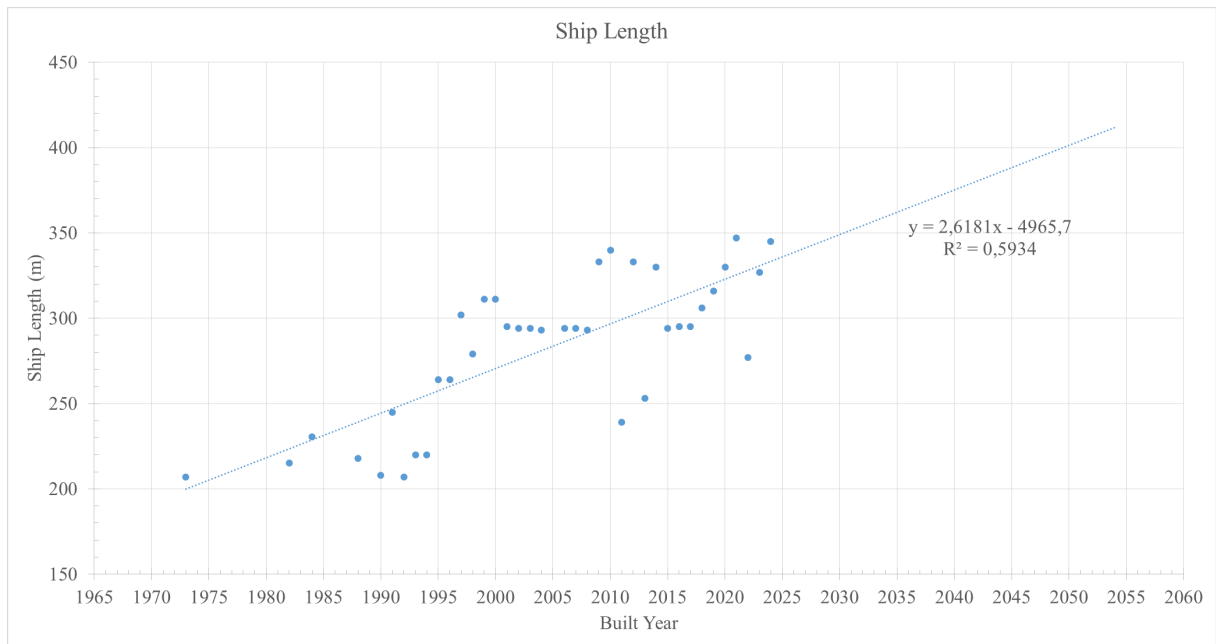


Fig. 2. Estimation of ship length

It is estimated that the ship draft will reach ~9.20 meters in approximately 2050 according to the linear regression curve fitted between ship draft and year of construction (Fig. 3). An annual increase of ~0.01 meters in ship draft is expected considering the ship draft increase by 0.20 meters in about 25 years.

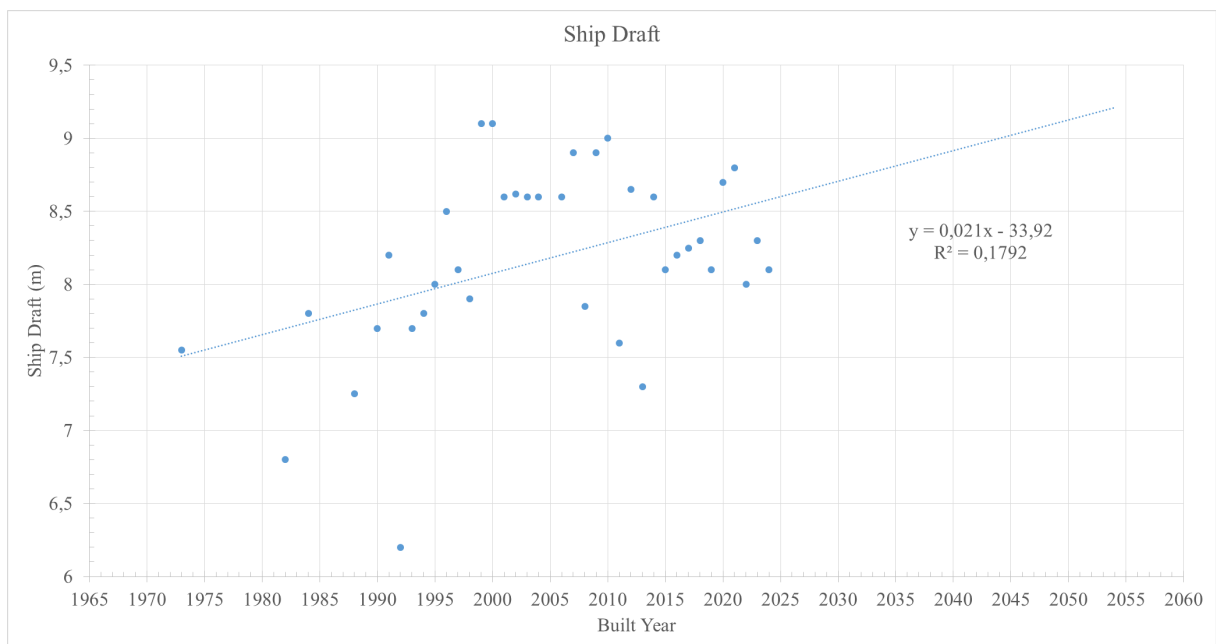


Fig. 3. Estimation of ship draft

The investment process (planning and construction) in a port in Türkiye takes approximately 10 years. It would be appropriate to study the investment plans of a port in 10-year periods considering this situation. Therefore, the demands of the ports in 10, 20 and 30 years from the current ship length and draft values (of the ports studied) were estimated by considering the increase in ship length and draft. Thus, the current infrastructure status of the ports was analyzed and investment needs were evaluated. In addition, investment needs are also presented in ports where the port infrastructure capacity has already been reached.

3. Results and Discussions

Some ports serve similar vessel lengths and drafts. There are 5 groups for ship length consist of Alanya-Marmaris, Antalya-Bodrum, Çanakkale-Trabzon, Çeşme-Dikili, İstanbul-İzmir-Kuşadası among the ports studied. The ship length is ~296 m in Alanya and Marmaris ports, ~316 m in Bodrum and Antalya ports, ~238 m in Çanakkale and Trabzon ports, ~231 m in Çeşme and Dikili ports, ~347 m in İstanbul, İzmir and Kuşadası ports in order to provide service to all ships. 4 groups are obtained as Alanya-Istanbul-Kusadası, Antalya-Marmaris, Bodrum-Izmir, Çanakkale-Çeşme-Dikili-Trabzon considering the vessel drafts. The ship draft is ~9.10 m in Alanya-Istanbul-Kuşadası ports, ~8.26 m in Antalya-Marmaris ports, ~8.65 m in Bodrum-Izmir ports, and ~7.96 m in Çanakkale-Çeşme-Dikili-Trabzon ports in order to provide service to all ships.

Taking into account the escalation in ship length and the ship lengths discerned from the investigation (Table 2):

- The anticipated requirements of Alanya port over the next 10, 20, and 30 years, starting from the current ship length of approximately 295 m, are estimated to be 305 m, 315 m, and 325 m, respectively.
- For Antalya and Bodrum ports, prognostications for the next 10, 20, and 30 years, based on the current ship length of around 316 m, indicate potential demands of 326 m, 336 m, and 346 m, respectively.
- Çanakkale port's projected needs over the same timeframe, beginning from the existing ship length of roughly 238 m, may reach 248 m, 258 m, and 268 m, respectively.
- For Çeşme and Dikili ports, the anticipated requirements over the next 10, 20, and 30 years, with the current ship length at about 231 m, could be 241 m, 251 m, and 261 m, respectively.
- İstanbul port's demands are expected to rise over the next 10, 20, and 30 years, starting from the current ship length of about 340 m, with estimations standing at 350 m, 360 m, and 370 m, respectively.
- Similarly, İzmir port's needs, based on the current ship length of 333 m, are forecasted to increase to 343 m, 353 m, and 363 m over the same periods.
- Kuşadası port's anticipated demands over the next 10, 20, and 30 years, beginning from the current ship length of 347 m, are estimated to be 357 m, 367 m, and 377 m, respectively.

- For Marmaris port, projections indicate potential demands of 307 m, 317 m, and 327 m in 10, 20, and 30 years, respectively, considering the existing ship length of around 297 m.
- Lastly, Trabzon port's anticipated requirements over the same periods, starting from the current ship length of approximately 236 m, are estimated at 246 m, 256 m, and 266 m, respectively.

Taking into account the rise in ship draft and the ship drafts derived from the study (Table 3), the anticipated demands for various ports were determined as follows:

- Alanya port's requirements in 10, 20, and 30 years from the current ship draft of 8.9 m could be estimated at 9.0 m, 9.1 m, and 9.2 m, respectively.
- For Antalya and Marmaris ports, based on the current ship draft of approximately 8.3 m, demands may escalate to 8.4 m, 8.5 m, and 8.6 m over corresponding periods.
- Projections for Bodrum port, with a present ship draft of 8.6 m, suggest demands of 8.7 m, 8.8 m, and 8.9 m in 10, 20, and 30 years, respectively.
- In Çanakkale port, with the current ship draft at around 8.0 m, estimations indicate demands of 8.1 m, 8.2 m, and 8.3 m over the same time frame.
- Likewise, for Çeşme, Dikili, and Trabzon ports, with a current ship draft of 7.8 m, demands could be estimated at 7.9 m, 8.0 m, and 8.1 m in 10, 20, and 30 years, respectively.
- Istanbul port's demands, based on the current ship draft of 9.0 m, are estimated to increase to 9.1 m, 9.2 m, and 9.3 m over corresponding periods.
- For Izmir port, with the current ship draft standing at 8.7 m, demands may rise to 8.8 m, 8.9 m, and 9.0 m in 10, 20, and 30 years, respectively.
- Lastly, for Kuşadası port, with a current ship draft of 9.1 m, demands are projected to be 9.2 m, 9.3 m, and 9.4 m over corresponding periods.

It is recommended to make development plans for Izmir, Alanya, Çanakkale, Marmaris and Dikili ports in the short term and Bodrum, Kuşadası ports in the long term according to the data compiled from the official pages of the ports and the estimations considering the current situation of the ports.

4. Conclusions

The evolution of cruise tourism since its inception in the late 1960s has been marked by steady growth, despite unprecedented challenges posed by the Covid-19 pandemic. The industry's resilience was evident in the rapid recovery witnessed in 2022, with expectations of surpassing pre-pandemic passenger numbers in the near future.

Analyzing cruise ship length and draft data for Turkish ports is crucial for effective development planning. Despite challenges in data availability and distribution fitting,

percentiles of ship lengths and drafts have been determined to guide planning efforts, providing insights into port accommodation capacity and anticipating future infrastructure needs.

Examining ship length and draft requirements for various ports reveals a diverse range of vessel sizes and draft depths necessary to accommodate incoming ships. Each port, from Alanya to Trabzon, presents unique planning considerations based on specific requirements and limitations.

Continuous monitoring and adjustment of development plans are crucial to align with evolving industry trends, such as the increasing size of cruise ships over time. Proactive measures, guided by thorough data analysis, are essential to ensure Turkish ports remain competitive and capable of meeting the demands of the growing cruise tourism industry.

Ship sizes are growing all over the world. The change in ship sizes in Turkey has been examined in the context of cruise ships, and there is an increase similar to the global trend in ship sizes.

Projections indicate a consistent trend of increasing ship sizes over time, with estimations suggesting ship length will reach 400 meters and ship draft approximately 9.20 meters by 2050. This underscores the need for forward-looking investment strategies, considering the lengthy planning and construction process for port infrastructure in Türkiye.

In conclusion, this study lays a foundation for informed decision-making in port development, offering valuable insights to optimize the efficiency and effectiveness of Turkish ports in serving cruise ships both now and in the future. By assessing regional effects on ship length and draft, the study provides valuable insights into the changing landscape of maritime transportation and proposes a pragmatic approach to investment planning.

Ultimately, the recommendations presented in this study serve as a valuable resource for guiding future infrastructure investments, ensuring the sustainable growth and competitiveness of Türkiye's maritime industry.

References

- [1] Bitiktas F. and Akpınar H., Türkiye'deki Kruvaziyer Limanlarının Mevcut Durumu, Potansiyeli ve Gelişimine Yönelik Öneriler, *III. Ulusal Deniz Turizmi Sempozyumu*, 2016.
- [2] BREA, *The Global Economic Contribution of Cruise Tourism 2013*, CLIA, Cruise Lines International Association, Washington, USA, 2014.
- [3] BREA, *The Global Economic Contribution of Cruise Tourism 2014*, CLIA, Cruise Lines International Association, Washington, USA, 2015.
- [4] BREA, *The Global Economic Contribution of Cruise Tourism 2015*, CLIA, Cruise Lines International Association, Washington, USA, 2016.
- [5] BREA, *The Contribution of the International Cruise Industry to the Global Economy in 2016*, CLIA, Cruise Lines International Association, Washington, USA, 2017.
- [6] BREA, *The Contribution of the International Cruise Industry to the Global Economy in 2017*, CLIA, Cruise Lines International Association, Washington, USA, 2018.

- [7] CLIA, *2019 Global Market Report*, Cruise Lines International Association, Washington, USA, 2019.
- [8] CLIA, *2022 Global Market Report*, Cruise Lines International Association, Washington, USA, 2022.
- [9] CLIA, *State of the Cruise Industry*, Cruise Lines International Association, Washington DC, USA, 2023.
- [10] CLIA, *State of the Cruise Industry Report*, Cruise Lines International Association, 2023.
- [11] Küçükosmanoğlu A., Türkiye'de Kruvaziyer Turizmi, *Destinasyon Pazarlamasında Turistik Ürün Çeşitlendirme ve Müşteri İlişkileri*, Ankara, Bidge Yayınları, 152-172, 2023.
- [12] General Directorate of Maritime Affairs, *Cruise Statistics*, Republic of Türkiye Ministry of Transport and Infrastructure, 2023. [Online]. Available: <https://denizcilikistatistikleri.uab.gov.tr/kruvaziyer-istatistikleri>. [Accessed 15 03 2024].
- [13] Su Ustünde, *Ship Schedules*, [Online]. Available: <https://www.suustunde.com/tr/contents/gemi-programlari.html?CatID=1>. [Accessed 11 02 2024].



Exploring the Spatial Distribution of Coastal Drainage Basins in Türkiye

Ozen Arli Küçükosmanoğlu

Burdur Mehmet Akif Ersoy University, Faculty of Engineering and Architecture, Department of Civil Engineering, Burdur, Türkiye

✉: okucukosmanoglu@mehmetakif.edu.tr, : 0000-0002-2119-8074

Received: 12.04.2024, Revised: 31.05.2024, Accepted: 01.07.2024

Abstract

Coastal regions are vital areas globally, serving as hubs for human habitation and economic activities. Water, being the fundamental resource for life, plays a crucial role in sustaining ecosystems and shaping coastal landscapes. The convergence of river systems in coastal zones underscores their significance in the hydrological cycle and aquatic biodiversity. However, managing these valuable yet vulnerable regions presents multifaceted challenges, necessitating robust management frameworks supported by monitoring and assessment tools. In Türkiye, a country with limited freshwater resources, the management of coastal zones is particularly complex due to increasing pressure on resources and land. This study examines the distribution and characteristics of river and coastal basins in Türkiye. Through spatial analyses on Geographical Information System and basin delineations with watershed modelling program, the study clarifies the regional differences and obstacles encountered by coastal provinces spanning the entirety of Türkiye's coastal borders. The results offer valuable understanding regarding the spatial dynamics of Türkiye's coastal areas with particular emphasis on the significance of Black Sea coastal basins and all coastal provinces. Firstly, river basin systems draining into the Black Sea constitute the majority of Türkiye's surface area. Although the Black Sea region covers only 14% of the total area, more than half of the country's surface area, excluding transboundary and endorheic basins, drains into the Black Sea. Similarly, the analysis of basin types reveals that coastal basins constitute approximately 18% of the drainage areas associated with our coastal waters, nearly one-fifth. This distinction between coastal basin and river basin boundaries differs from the traditional zoning approach in river basin management and coastal area management plans in Türkiye. Consequently, it is anticipated that this spatial evaluation, which has brought a new perspective, will significantly contribute to addressing management challenges, especially the studies that will be evaluated together with population and resource use.

Keywords: River Basin, Coastal Basin, Coastal Zone Management.

1. Introduction

Coastal regions are geographical areas in demand all over the world. As is widely acknowledged, water stands as the most essential resource for sustaining life. During hydrological cycle, water feeds aquatic ecosystems and creates valuable habitats throughout its movement from land to sea. The final regions traversed by the majority of river systems before reaching the oceans are the coastal zones, which have undergone formation and molding processes spanning hundreds of thousands of years. Our planet is a water planet but freshwater content is around 0.4%. Only 1.6% of this amount is river discharges [1]. Despite the relatively low volume transported by rivers, their influence on coastal processes and significance for aquatic life in marine environments is substantial. Coastal areas are very valuable due to the presence of water, the diversity of their resources, and the fact that they are a gateway to the sea that allows trade, most of which is carried out by maritime transport. Ancient cities and ruins prove that coastal zones were always appealing. Water, food, and agricultural natural resources; fisheries and marine transport are significant ones [2, 3].

When we compare the ratio of overall coastal area to total land area and ratio of population of corresponding regions, the result reveals that the coastal population exceeds many folds of



inland regions. More than half of the world population lives near coast from 100 km from the shore [4-8]. Two third of mega cities of the world and most of the capital of countries has a sea border located in coastal zones [2, 7, 9].

All these circumstances complicate the management of these vulnerable and valuable regions. Sound management practices show that; the tools, legislations and different organisational structures needed in coastal zone management. Monitoring and assessment tools are essential to support all these management and decision-making systems, particularly in provinces along the coastline, which encompass extensive coastal areas.

According to the definition, the coastal area is "the land and sea areas bordering the shoreline." This terminological definition, however, did not account for the resources and solutions required for integrated management, it gained a more adaptive / flexible borders in the process until the 1990s. The coastal zone is defined as "The land-sea interface where the land is influenced by marine processes and the sea is affected by terrestrial processes" by the Coastal Engineering Manuel [10]. If the definition of the coastal zone in Coastal Zone Management plans is flexible based on the problem definition and solution focus, integration and ecosystem approach can be achieved. For this reason, the boundaries of the area covered for each project vary in Integrated Coastal Zone Management (ICZM) Plans. There are plans for regional seas and countries, as well as those focused on more specific ecosystem problems. In national plans, administrative boundaries such as geographical regions and provincial borders are considered. Basin management plans typically address large river basins. This may overshadow the importance of coastal basins —the primary region at the land/sea interface where processes impact each other.

Examining the existing literature reveals a scarcity of studies delving into the significance of coastal basins and their role in different processes. For instance, Simms et al. conducted research on erosion management, where they modelled a small basin in Lake Wollumboola, Australia, to assess soil erosion dynamics. The research highlighted the influence of coastal basin degradation and land use practices on soil erosion dynamics [11].

In the research conducted by another team [12, 13], coastal basins are calculated separately and their impacts are analysed. In the first study, spatial findings similar to those in our research stand out. The calculated spatial coastal basin values here have also been evaluated together with population and other geographical information. In the study, near-coastal unmonitored catchments of Baltic Sea Drainage Basin are presented. 634 sub-drainage basins and their various spatial aggregations are characterized in terms of population; land cover, drainage density, and slope were studied. They indicate that, 13% are is unmonitored near-coastal areas which inhabit 24% of the total basin population. For Sweden, this numbers were calculated as 20% of total catchment area of Sweden with a population of 55% [12]. The second study of the team examined the near-coastal unmonitored drainage basins have impact on coastal water quality conditions. They state that, coastal basins contain a considerable amount of residential areas and population as compared to the inland areas and large river basins. With this study, nutrient and pollutant mass loading to the sea shows a pollution magnitude similar to or greater than monitored river loads. [13].

Another study conducted in South America also reveals the importance of coastal basins. Marquez et al. [14] evaluated the environmental impacts in the basins located on the Atlantic coast of South America. Within the scope of management studies, they evaluated the effectiveness of treating coastal basins as separate geographical units. The study revealed that, apart from the usual river basin management framework, small water resource basin studies can be effective both for determining habitat loss and aquatic ecosystem degradation, and for regaining fauna in economically manageable small basins.

In recent years, there have been many studies in the literature on low elevation coastal zones involving the determination of global warming and its effects. In one study [15], Soboyejo and colleagues emphasizes the importance of drainage basins size selection in the long-term water resource management and planning of coastal basins. Study reveals that the drainage behaviour in these basins is related to the land subsidence, past management practices, and climate variability of the area. The findings of this research suggest that climatological variations and land usage practices have a substantial impact on the drainage patterns observed in coastal basins. Specifically, factors such as precipitation, evapotranspiration, drought occurrences, and water availability exhibit closer correlations in coastal basins compared to inland areas.

Türkiye is a peninsula and has a strategically important location. In addition to its extensive river basins, the smaller riverine discharge basins and coastal basins contribute to Türkiye's water resources, enriching the country's water assets. This is significant considering Türkiye's status as a country with limited water abundance, with an annual average rainfall of 574 mm [16]. This average annual rainfall is less than the world average. Therefore, managing these limited resources in this vulnerable and attractive geographical area poses challenges in Türkiye as well. The pressure on the resources and sectors on the coastal regions of Türkiye is increasing every day. For this reason, the integrated management approach is gaining importance. It is thought that the comparative areal evaluations obtained in the study will shed light on the needs and priorities of our country in the field of coastal zone management. Therefore, water drainage basins, especially coastal small basins are currently receiving attention in terms of management.

In our study, the river and coastal basins in Türkiye were examined according to their sizes, locations and discharging sea area. The spatial evaluation of the coastal basins was also evaluated according to the geographical and marine regions. The coastal basins along the Mediterranean, Aegean, Marmara, and Black Sea shorelines were analysed in terms of their sea discharge. Regional variations were identified and discussed. Furthermore, differences in basin area based on Türkiye's Nomenclature of Territorial Units for Statistics (NUTS) and the corresponding discharging sea areas were delineated.

2. Methodology

In this study, first of all Türkiye's geographical regions were transferred to Geographical Information System (GIS) environment using level information of NUTS of Türkiye. Then, the basin dataset of the regions where Türkiye is located were downloaded from the world Georeferenced global Dams And Reservoirs - Drainage Topology and Catchment database (GeoDAR-TopoCat) data [17,18]. The river basin data of Türkiye were added to our database (DB). Since the river basin data only covers large basins, delineation of smaller basins was made using 30 m resolution Shuttle Radar Topography Mission (SRTM) 1 Arc-Second Digital Elevation Model (DEM) data in those areas. These analyses were performed using the Aquaveo Watershed Modeling System (WMS). The flowchart of the study is presented in Fig. 1.

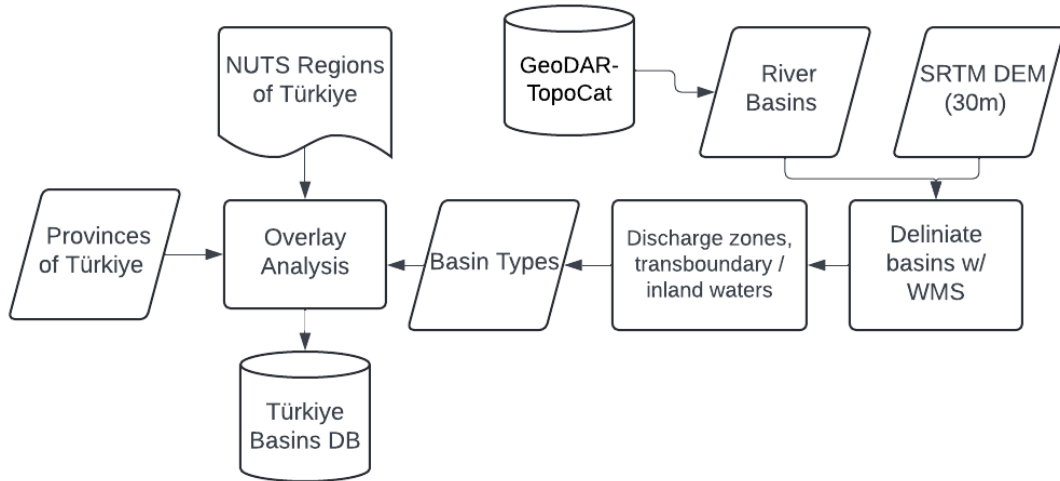


Fig. 1. Study flowchart

After these determinations, the basin areas outside the perennial rivers with continuous flow (intermittent and ephemeral streams) were included in the coastal basins. With this delineation, inland basin regions were also more clearly separated and included into our GIS basin database. After this work, the basins were classed into the seas where they spill into and the geographical regions where they are included in. Therefore, the areal assessments could be possible to complete so that an assessment could be made about the coastal basins and their distribution. Here, analysis criteria were selected to extract river basins of certain sizes. Fig. 2 shows the coastal and river basins of Türkiye and their distribution. The basins indicated in white in the figure are the basins of external/trans boundary waters whose discharge zones are outside our country. The basins in grey are coastal basins and the basins in light grey are the basins of our rivers with a continuous flow regime above a certain size.

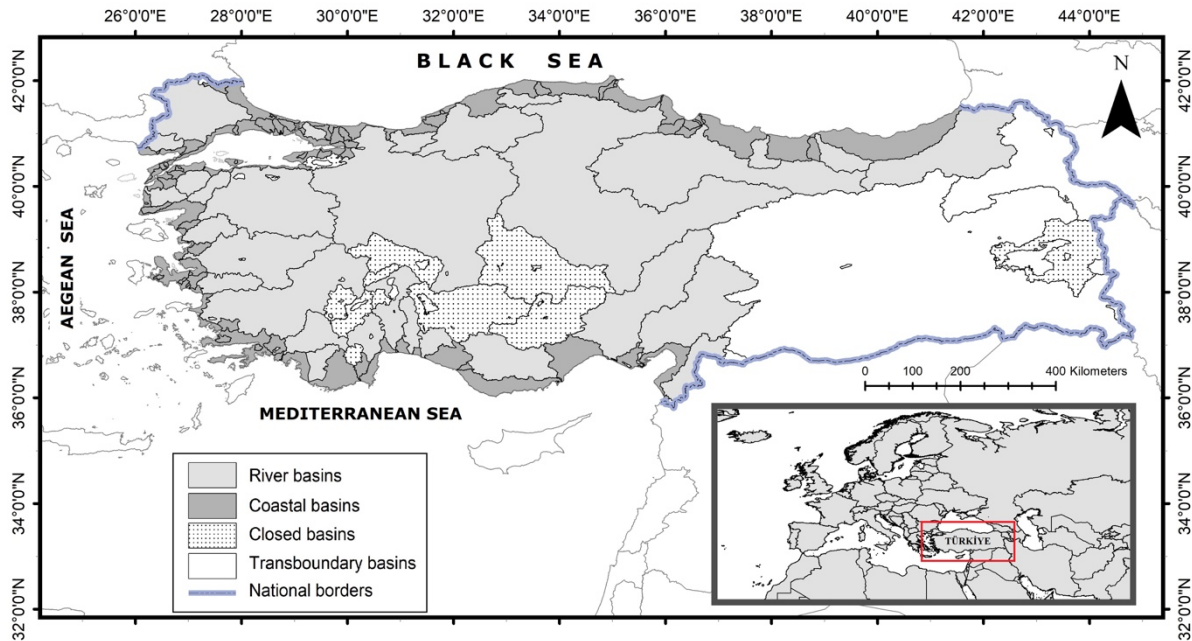


Fig. 2. Study area and basin types

The resulting basin areas were processed in a way to differentiate coastal basins, according to the flow regime. Perennials are distinguished from intermittent and ephemeral streams. The

data produced in the whole study were transferred to the GIS. Corrections for all lake areas, is also obtained from GeoDAR-TopoCat data, were made on the GIS and the lake surface areas were subtracted from basin areas. Each basin was named and various attribute information were entered into the database.

The distribution of the river basins, the boundaries of which were determined and the attributes of which were entered, according to the seas they discharge into, was also determined and it was determined which rivers and coastal basins discharge into which marine areas. For the geographical region evaluations, level 1 and 2 geographical regions of the NUTS regional system, which was adopted by the Council of Ministers Decree dated 2001 were used [19]. Although it is very close to the geographical regions we are used to. Similarly, the distribution of basins included into the coastal provinces was also analysed and the findings are presented in the results section.

3. Distribution of Basins and Their Types

Our country is surrounded by seas on three sides. Evaluations of river basins draining into the sea outside our borders have been provided in tables, but for a clearer understanding of the overall distribution, they have not been color-coded on the maps. These basins include the areas of two major rivers, the Euphrates and Tigris, originating in the eastern parts of our country and flowing into the Persian Gulf, as well as the river basins draining into the Caspian Sea and enclosed/internal basins (

Fig. 3). The total area of these external basins constitutes approximately 27% of our land area. Closed basins and lake basins have also been separately calculated and presented in the tables (Table 1).

Enclosed/internal basins comprise 10% of Türkiye's land area (Table 1). These areas, which also include lake basins, have not been color-coded in Fig. 3.

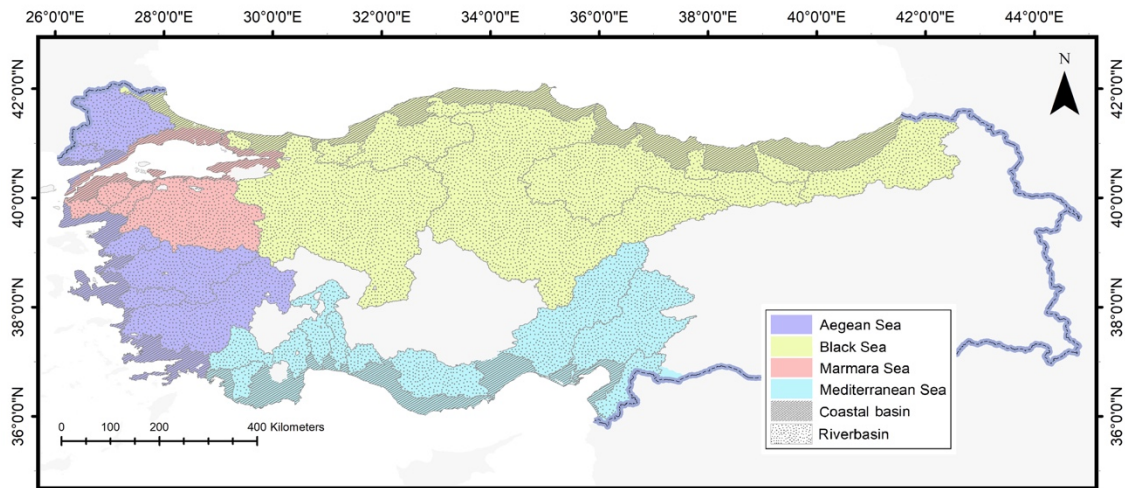


Fig. 3. The distribution of coastal and river basins based on the seas into which they drain

Table 1. Distribution and percentage area coverage of basin types across various sea regions being drained

	Closed Basins	Transboundary Basins	River Basins	Coastal Basins	%Sea Region Poured
<i>Aegean Sea</i>	0	0	15.8	18.9	10.3
<i>coastal **</i>				13.1	1.5
<i>stream channel *</i>	0	0	15.8	5.8	8.8
<i>Black Sea</i>		0.1	56.2	43.2	34.0
<i>coastal **</i>	0	0	0	37.1	4.3
<i>stream channel *</i>		0.1	56.2	6.1	29.7
<i>Marmara Sea</i>	0	0	7.4	11.7	5.2
<i>coastal **</i>				7.7	0.9
<i>stream channel *</i>	0	0	7.4	4.0	4.3
<i>Mediterranean Sea</i>		0.5	20.7	26.3	13.8
<i>coastal **</i>	0	0	0	25.2	2.9
<i>stream channel *</i>		0.5	20.7	1.1	10.9
<i>Inland</i>	100	0	0	0	10.2
<i>closed basin</i>	100				10.2
<i>Caspian Sea</i>	0	14.1	0	0	3.8
<i>stream channel</i>		14.1			3.8
<i>Persian Gulf</i>	0	85.3	0	0	22.8
<i>stream channel</i>		85.3			22.8
<i>Grand Total</i>	100	100	100	100	100

* Perennials streams

** Ephemeral and intermittent streams

The distribution of basin types across various sea regions in terms of percentage area coverage is presented in Table 1. In the Black Sea, is the largest area of sea being drained, river basins make up 56% and coastal basins 43%, totaling 34% overall. In the Mediterranean Sea, river basins cover 21%, coastal basins 26%, totaling 14%. For the Aegean Sea, river basins account for 16%, coastal basins for 19%, totaling 10%. The Marmara Sea has 7% coverage from river basins, 12% from coastal basins, totaling 5%. The Persian Gulf is dominated by transboundary basins, Euphrates and Tigris, covering 85%, totaling 23% of Türkiye. The Caspian Sea shows 14% coverage from transboundary basins, totaling 4%. Upon refining our analysis and omitting inland basins and rivers that do not discharge into the sea from our borders, it becomes evident that 54% of Türkiye's total surface area drains into the Black Sea region. In the context of coastal basins, 37% of the surface area lies along the Black Sea coasts, followed by 22% along the Mediterranean coasts.

The provided Table 2 shows the distribution of various basin types across NUTS regions. Central Anatolia has the highest proportion of closed basins, accounting for 62%, followed by Eastern Anatolia at 17%. In terms of transboundary basins, Eastern Anatolia is predominant, with these basins comprising 81% of the region and 58.8% of all transboundary basins in Türkiye, primarily due to the Euphrates and Tigris river basins. The Mediterranean region has the highest percentage of river basins at 14%, encompassing 65% of the region. In the Aegean Region, river basins and coastal basins cover 75% and 15% of the area, respectively. Over one-third of Türkiye's coastal basin area is located in the Black Sea region (37%), where the topography features mountains running parallel to the sea. The Black Sea region accounts for only 14% of Türkiye's total surface area. However, when excluding transboundary and

endorheic basins, it is evident that more than half of the country's surface area drains into the Black Sea.

Although the Mediterranean and the Marmara regions account for 11.4% and 12.5% of Türkiye's total area respectively, it is evident that they collectively encompass half of Türkiye's coastal basin area. Together with the Black Sea region, these three regions host 85% of all Turkish coastal habitats, underscoring their significance. Overall, the Table 2 demonstrates a diverse distribution of basin types across various NUTS regions, with each region contributing proportionally to both the total area of each basin type and the total area of the region. In the table, basin types are evaluated numerically in two distinct columns. The column marked with a right arrow shows the percentage distribution of each basin type within that geographical region. The column indicated by the downward arrow presents the ratios of the basin type surface area within that geographical region to the total surface area of all basin types.

Table 2. The distribution of basin types across geographical regions

NUTS Regions	% Coverages								Total →→	
	Closed Basins		Transboundary Basins		River Basin		Coastal Basins			Region/TR Area
	↓*	→**	↓	→	↓	→	↓	→		↓
The Mediterranean	9.5	8.5	0.8	1.8	14.4	65.0	24.4	24.6	11.4	100
Eastern Anatolia	17.0	8.9	58.8	81.1	3.7	9.9	0.1	0.1	19.3	100
Aegean	10.2	9.1	0.0	0.0	16.8	75.6	15.2	15.3	11.5	100
Southeastern Anatolia	0.0	0.0	35.6	96.1	0.7	3.9	0.01	0.01	9.9	100
Central Anatolia	61.9	29.7	4.7	5.8	26.6	64.4	0.2	0.1	21.3	100
Black Sea	0.0	0.0	0.1	0.2	19.1	69.8	36.7	30.0	14.1	100
Marmara	1.4	1.1	0.1	0.3	18.6	76.9	23.4	21.7	12.5	100
Total ↓↓	100		100		100		100		100	

*↓ Spatial proportion among basin types

**→ Basin type ratio of geographical region

The drainage basins that contribute to the Black Sea's hydrology extend into the Central Anatolia, Aegean, and Marmara Regions of our territory. Conversely, within the Aegean and Mediterranean Regions, hydrological inputs primarily arise from local catchment areas. Notably, the contributing drainage basins to the Black Sea stem from Türkiye's prominent rivers, namely the Kızılırmak, Yeşilirmak, and Sakarya Rivers, with their respective spatial extents illustrated in Fig. 4.

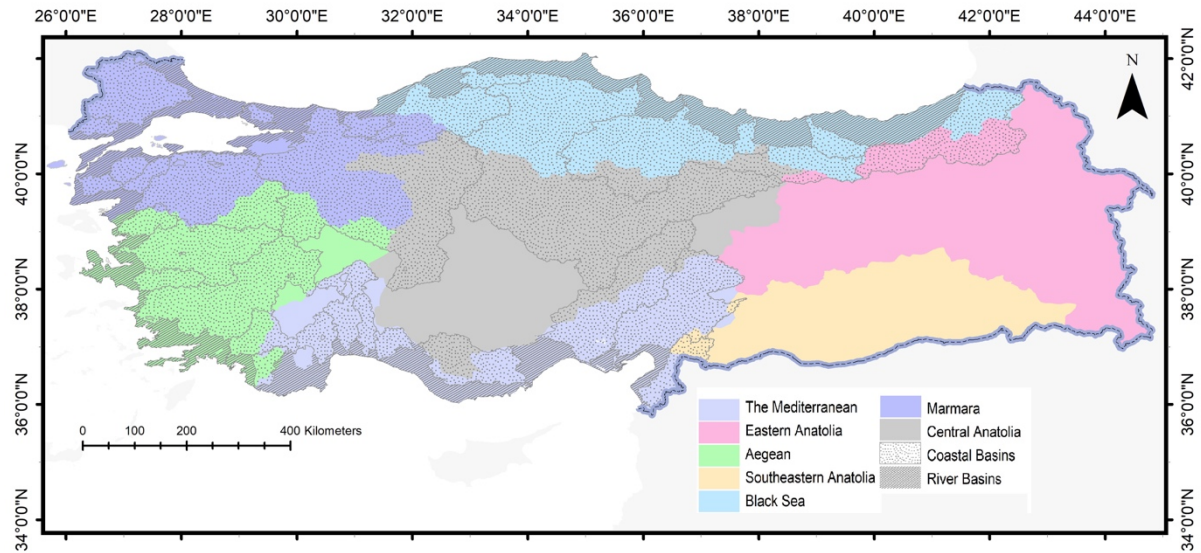


Fig. 4. The distribution of river and coastal basins according to NUTS geographical regions

Table 3. Basin type percentage distributions of coastal provinces

Area Distribution %	Closed Basins	Trans-boundary Basins	River Basin	Coastal Basins	Coastal Province Area %
Adana	0	0	2.99	1.89	1.76
Antalya	1.74		2.16	11.51	2.62
Artvin	0	0.1	1.69	0.66	0.97
Aydın			1.84	0.72	1.03
Balıkesir	0	0	2.96	2.75	1.84
Bartın			0.05	2.4	0.3
Bursa	1.26	0	2.16	0.76	1.33
Çanakkale			1.26	5.09	1.24
Düzce	0	0	0.53	0.42	0.32
Edirne			1.41	0.64	0.8
Giresun	0	0	0.76	4.5	0.91
Hatay		0.09	0.85	2.16	0.71
İstanbul	0	0	0.2	5.15	0.7
İzmir			1.74	5.71	1.56
Kastamonu	0	0	2.51	3.28	1.67
Kırklareli		0.13	1.12	1.88	0.83
Kocaeli	0.02	0	0.11	3.28	0.44
Mersin	0.35		1.93	8.68	2.03
Muğla	0	0	1.26	8.5	1.63
Ordu			0.53	4.24	0.76
Sakarya	0	0	1.11	0.4	0.62
Samsun			1.18	5.62	1.26
Sinop	0	0	0.62	3.53	0.73
Tekirdağ			1.08	2.15	0.8
Trabzon	0	0	0.01	5.17	0.6
Yalova	0.02			0.86	0.1
Zonguldak	0	0	0.39	1.8	0.41
Rize			0.02	4.25	0.5
Percentage of Basin Types in Coastal Provinces Relative to Türkiye's %	3.4	0.32	32.49	97.98	28.49

The evaluation results conducted on a coastal province basis using overlay analysis are presented in Table 3. In this table, coastal province area gives the percentage of coastal provinces' land area compared to the total land area of Türkiye. Similarly, the values in basin type columns indicate the percentage of these basin types within coastal provinces relative to their total areas across Türkiye. Upon examining the values therein, it is evident that while the percentage distribution of river basin areas is relatively small, coastal provinces exhibit a notably higher distribution of coastal basin areas. Coastal provinces constitute 28% of the total surface area of Türkiye. The proportion of river basin area in coastal provinces to the total river basin area of Türkiye is 32%, whereas the proportion of coastal basin area in coastal provinces to the total coastal basin area of Türkiye naturally stands at 98%. The provinces with the largest river basin area proportions are Adana, Balıkesir, Kastamonu, and Antalya, respectively. In terms of coastal basin proportions, the ranking is as follows: Antalya, Mersin, Muğla, İzmir, Samsun, Trabzon, and İstanbul. In Table 3, data bars are gradient-filled to enhance the readability of the table. Here, in addition to the importance of Antalya, Mersin and Muğla provinces as we know, it has been revealed that they are important coastal provinces in terms of coastal basins. In the studies to be conducted in these provinces in terms of coastal zone management, it is seen that small coastal basins are more important than the river basin considered in traditional management practices.

4. Discussion

Coastal zones have become increasingly important since the 1970s due to on-going destruction and anthropogenic pressures. Efforts in coastal zone management and river basin management aim to mitigate these adverse impacts. While river basin management primarily focuses on water resources, ICZM necessitates a more specialized management approach due to its dependency on various resources. Coastal zones are characterized by diverse uses and denser populations compared to inland areas worldwide. Establishing such smaller coastal catchments/ basins defined in this study can facilitate more effective governance.

When we look at the scope of the ICZM spatial plans or basin-based plans carried out in Türkiye, it is seen that coastal basins are not specifically mentioned. In these plans, it is seen that a framework is determined according to administrative units or regions or basins. Basin management plans consist of 26 basins delineated according to the hydrological characteristics of the major river basins and their surrounding regions. The plans rely on existing structures for decision-making systems, avoiding the need for specialized legislation and new management infrastructure. However, according to the principles of integrated and ecosystem-based management, dynamic and unique coastal regions require flexibility and adaptability in decisions.

The novelty of this study is to reveal the findings that will pave the way for the special structure of coastal basins to be included in monitoring and decision-making processes. Analysing the distinctions of coastal basins within the context of provincial, drained, or geographical regions reveals deficiencies in current approaches. The primary issue is the need to conduct monitoring studies on carrying capacities and environmental pollution in coastal basins. Conducting detailed studies on a larger geographical scale or on a river basin basis in coastal areas with population and pollution pressures, as demonstrated by Marquez et al., may enhance efficiency in terms of both time and cost.

This distinction is becoming more apparent in various monitoring and evaluation aspects of coastal zone management studies worldwide. The proportion of coastal basins to the total surface area in our country is significant, close to one-fifth at 18%, when assessed together with the streams drained into our seas. In the study of the Baltic Sea [12], which is an inland

sea like the Black Sea, the spatial percentage of coastal basins shows a similarity with Türkiye. The separate evaluation of coastal basins in terms of environmental effects reveals pressure discrepancies previously unnoticed. Considering population distribution and densities in coastal regions, similar pressure situations are evident in our country [20, 21]. This study sheds light on overlooked areas in future planning and strategy studies, or adaptive renovation of former projects. Monitoring and decision-making processes are successive processes. It has also been seen in literature that these coastal basins, which appear smaller compared to the basin and provincial areas, do not participate in the monitoring evaluation processes in the usual processes in the world.

Management entities are tasked with assessing and mitigating the utilization of resources, pollution, and pressures, especially concerning water resources. However, in the basin management plans made in our country [22], it is not investigated how coastal basins have an impact on environmental degradation [23]. When we look at the Integrated Coastal Zone Plans of Directorate General of Spatial Planning of Ministry of Environment, Urbanisation and Climate Change [24], it is seen that the plans do not go far beyond spatial planning. National strategic plan studies conducted for water quality monitoring between 2012-2023, as well as those conducted for compliance with the implementation of the water framework directive, are observed to have insufficient focus on coastal basins. The examples presented in the literature have shown both the difference of water resource dynamics in coastal basins and the fact that environmental pressures can be as intense in coastal basins as in inland ones [11, 13, 14, 15].

5. Conclusions

The coastal regions of our country, strategically positioned and bordered by seas on three sides, face escalating pressure on their resources and sectors. This heightened importance underscores the growing significance of adopting an integrated management approach. Comparative analyses between coastal and inland areas starkly reveal the substantial difference, with coastal populations far exceeding those of inland regions. A closer examination of coastal basins' areal coverage emphasizes the criticality of addressing coastal management issues in provinces directly affected. The comparative spatial assessments garnered from the study are anticipated to illuminate the needs and priorities of our country in coastal zone management.

For instance, the Mediterranean coastlines alone occupy 24% of Türkiye's land area, accommodating diverse human activities and ecological habitats. Particularly, the Black Sea basin receives runoff from approximately 54% of the country's total surface area, underscoring the significant role of rivers such as the Kızılırmak, Yeşilirmak, and Sakarya in the region's hydrological dynamics. Considering the Black Sea region, which is adjacent to an environmentally vulnerable inland sea and its critical habitats, a coastal basin perspective clarifies regional environmental pressures and hazards such as erosion and flooding, while also emphasizing the importance of addressing marine pollution within broader river basin management efforts. Excluding inland and transboundary basins, the proportion of coastal basins to the total surface area is 18%. Therefore, The Mediterranean and Marmara regions are notably more important as their percentages of coastal basins exceed their surface area proportions. This highlights the need for attention to settlements at coastal area, population dynamics of the coastal regions, and carrying capacity determinations in these regions.

Further provincial-level analysis unveils the disproportionate contribution of coastal provinces to coastal basin coverage compared to river basins, with these areas often extending significantly into provincial borders. Notably, provinces like Antalya, Mersin, Muğla, İzmir,

Samsun, Trabzon, and Istanbul emerge as pivotal centers, boasting the largest populations and economic activities. This comprehensive assessment offers valuable insights into Türkiye's coastal zones' hydrological dynamics and management challenges, guiding future strategies for sustainable coastal development and resource management. Adopting an integrated coastal zone approach and tailoring decisions to specific regional needs will undoubtedly yield more effective outcomes when addressing the management issues of these provinces.

References

- [1] Garrison, T. S., *Oceanography: An Invitation to Marine Science*. Cengage Learning, 8th Edition, 2012.
- [2] Cicin-Sain, B. and Knecht, R., *Integrated Coastal and Ocean Management Concepts and Practices*, Washington D.C.: Island Press, 1998.
- [3] Westmacott, S., Where should the focus be in tropical integrated coastal management?, *Coastal Management*, 30(1), 67-84, 2002.
- [4] Sorensen, J. C., and McCreary, S. T., *Institutional Arrangement for Managing Coastal Resources and Environments*, Washington, DC: National Parks Service, U.S. Department of Interior, 1990.
- [5] UNCED, Agenda 21 Chapter 17: Protection of the oceans, all kinds of seas, including enclosed and semi-enclosed seas, and coastal areas and the protection, rational use, and development of their living resources, *Report of the United Nations Conference on Environment and Development 2*, Rio de Janeiro: UNGA (United Nations General Assembly), 1992.
- [6] Cicin-Sain, B., Sustainable development and integrated coastal management. *Ocean and coastal management*, 21(1-3), 11-43, 1993.
- [7] Clark, J., *Integrated Management of Coastal Zones*, Rome, Italy: Food and Agricultural Organisation of the United Nations, 1992.
- [8] Creel, L., *Ripple Effects: Population and Coastal Regions*. Washington, DC: Population Reference Bureau, 2003.
- [9] WCC, Preparing to meet the coastal challenges of the 21st century, *Report of the World Coast Conference*, Noordwijk: The Hague: Ministry of Transport, Public Works and Water Management, 1994.
- [10] U.S. ARMY Corps of Engineers. *Coastal Engineering Manual*. Engineer Manual 1110-2-1100, USACE: Washington, DC, USA, Volume (1-4), 2011.
- [11] Simms, A. D., Woodroffe, C. D., and Jones, B. G., Application of RUSLE for erosion management in a coastal catchment, *University of Wollongong, Faculty of Science - Papers (Archive)*, southern NSW, 2003.
- [12] Hannerz, F., and Destouni, G., Spatial characterization of the Baltic Sea Drainage Basin and its unmonitored catchments, *AMBIO: A Journal of the Human Environment*, 35-5, 214 – 219, 2006. doi:10.1579/05-A-022R.1.

- [13] Destouni, G., Hannerz, F., Prieto, C., Jarsjo, J., and Shibuo, Y., Small unmonitored near-coastal catchment areas yielding large mass loading to the sea, *Global Biogeochem. Cycles*, 22, GB4003, 2008. doi:10.1029/2008GB003287.
- [14] Marques, M., Costa, M.F., Mayorga, M.I.O., and Pinheiro, P.R.C., Water Environments: Anthropogenic Pressures and Ecosystem Changes in the Atlantic Drainage Basins of Brazil, *AMBIO: A Journal of the Human Environment* 33(1), 68-77, 2004. <https://doi.org/10.1579/0044-7447-33.1.68>
- [15] Soboyejo, L.A., Giambastiani, B.M.S., Molducci, M., Antonellini, M. Different processes affecting long-term Ravenna coastal drainage basins (Italy): implications for water management, *Environ Earth Sci* 80, 493, 2021. <https://doi.org/10.1007/s12665-021-09774-5>
- [16] Hadi, S.J., Tombul, M. Long-term spatiotemporal trend analysis of precipitation and temperature over Turkey, *Meteor. Appl*, 25, 445–455, 2018.
- [17] Wang, J., Walter, B. A., Yao, F., Song, C., Ding, M., Maroof, A. S., Zhu, J., Fan, C., McAlister, J. M., Sikder, M. S., Sheng, Y., Allen, G. H., Crétau, J.-F., and Wada, Y., GeoDAR: georeferenced global dams and reservoirs database for bridging attributes and geolocations. *Earth System Science Data*, 14, 1869-1899, 2022. <https://doi.org/10.5194/essd-14-1869-2022>.
- [18] Sikder, M. S., Wang, J., Allen, G. H., Sheng, Y., Yamazaki, D., Song, C., Ding, M., Crétau, J.-F., and Pavelsky, T. M., Lake-TopoCat: A global lake drainage topology and catchment dataset. *Earth System Science Data Discussion, in review*, 2022. <https://doi.org/10.5194/essd-2022-433>, 2023.
- [19] KA, Kalkınma Ajansı Kalkınma Planlamasında İstatistiki Bölge Birimleri Sınıflandırması, (22 Aug 2023). [Online]. Available: <https://ka.gov.tr/sayfalar/kalkinma-planlamasinda-istatistiki-bolge-birimleri-siniflandirmasi--24>
- [20] Sağdıç, K.E., Türkiye kıyı bölgelerinin yıllara göre nüfus değişimi, Master's Thesis, Mehmet Akif Ersoy University, 2024.
- [21] Küçükosmanoğlu, Ö. A., Küçükosmanoğlu, A., & Sağdıç, K. E., Türkiye Kıyı Bölgeleri Nüfus Yoğunluğunun İncelenmesi. III. *Uluslararası Mesleki ve Teknik Bilimler Kongresi*. 4, s. 2674-2676. Gaziantep: UMTEB, 2018.
- [22] Tarım ve Orman Bakanlığı, Su Yönetimi Genel Müdürlüğü, Nehir Havza Yönetim Planları Web sayfası. (09.05.2024) <https://www.tarimorman.gov.tr/SYGM/Sayfalar/Detay.aspx?SayfaId=49>
- [23] Öztürk, S., Tönük, G.U., Gülgün, B., Türkiye’de Havza Yönetimi ve Yönetim Planı Yaklaşımları , *Ziraat Mühendisliği*, 361(1), 2014.
- [24] Mekansal Planlama Webpage, T.C. Çevre, Şehircilik ve İklim Değişikliği Bakanlığı, Directorate General of Spatial Planning. Integrated coastal area plans. 10.05.2024. <https://mpgm.csb.gov.tr/planlar-ve-projeler-i-84130>